Doctoral Dissertation (Shinshu University)

Mechanism of preferential etching of boron-doped diamond electrodes by steam or CO_2 activation

March 2014

Junfeng Zhang

Contents

Chapter 1

General introduction

1.1. Synthetic diamond film

1.1.1. Diamond

Diamond is a well-known gemstone. Due to the outstanding properties, such as the hardness and chemical stability, diamonds find extensive applications in industry. Diamond structure is composed of tetrahedral bonded carbon atoms in a covalent network lattice (sp^3), which is a variation of the face centered cubic structure (**Fig. 1.1**).

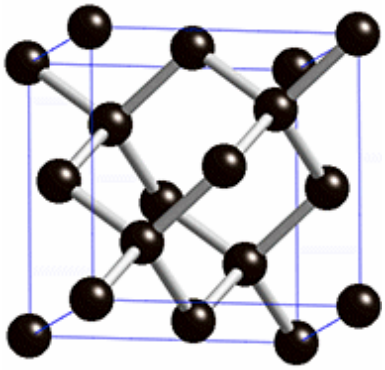

Fig. 1.1. Face centered cubic structure of diamond [2].

The ideal models of mono-hydrogenated diamond {100} and {111} surfaces are shown in **Fig. 1.2**. The (2×1) monohydride is the stable state of the diamond {100} (**Fig. 1.2**). The {111} surface is constituted by 6-atom hexagonal rings and adjacent atoms are arranged alternatively displaced upward and downward from the plane. The different surface C-C length, as shown in **Fig. 1.2**, leads to different surface reactivity.

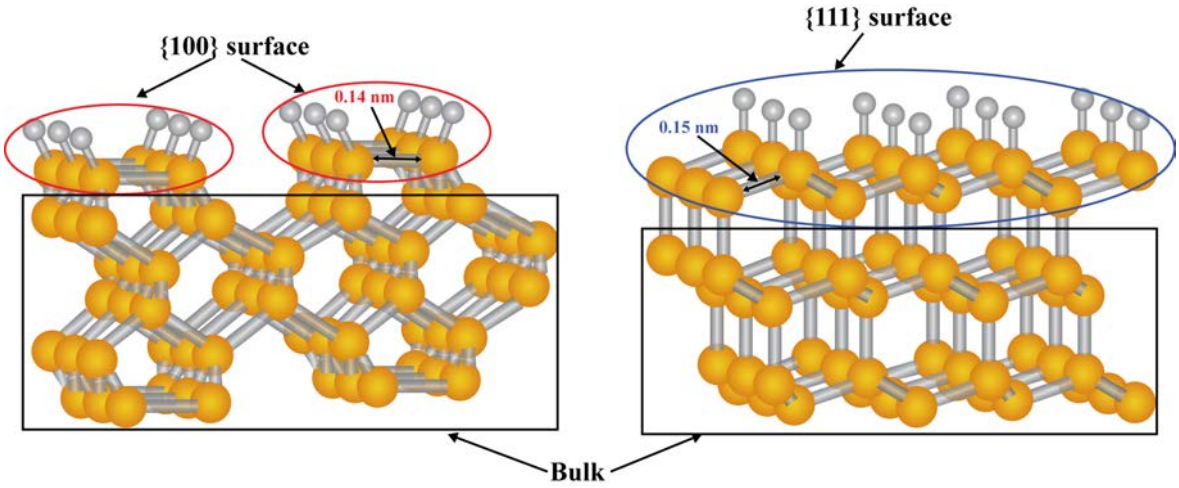

Fig. 1.2. Side view of mono-hydrogenated diamond {100} (left) and {111} (right) surfaces.

1.1.2. Synthesis of diamond film

Diamond was artificially synthesized under high-pressure and high-temperature in 1955 [1]. In this process, graphite mixed with transition-metal (Fe, Ni, Co, etc.) catalyst powders is subjected to high-pressure and high-temperature (300 kbar, 2200 - 3000 K) [2]. The role of catalyst is to decrease the activation energy of the conversion of graphite to diamond for ensuring them to reconstitute as diamond [3]. Chemical vapour deposition (CVD) provides a way for diamond synthesis by converting a gas phase carbon-containing species into diamond crystallites at lower pressure compared to the high-pressure high-temperature technique [4-6]. CVD diamond has been realized for technological applications since it can be synthesized as a thin film, chemically bonded to a nondiamond substrate [3].

Hot filament-assisted CVD (HFCVD) is the most common method for diamond film deposition due to its low-cost and simplicity. In this method, a tungsten filament heated at 2000 °C, which is placed above the substrate heated at ~700 - 1000 °C, is used for thermal

decomposition of carbon containing species. A mixture of methane (CH_4) and hydrogen (H_2) gas is often used as the carbon source. During deposition, atomic hydrogen is believed to remove the graphitic carbons and makes it possible to selectively grow diamond. The growth rate of diamond on the substrate is 0.2~2 μm h^{-1} [3]. The hot filament-assisted CVD method allows the production of electrodes with large surface areas (up to 0.3 m^2) for industrial applications, but contaminations from the filament can not be fully avoided and contains a fraction of sp^2 carbon impurity. The effect of heating temperature, pressure, gas source and substrates is discussed in detail in literature [5].

1.1.3. Boron-doped diamond film

Hydrogenated diamond was found to have high surface conductivity in 1989 [7], and is known as surface transfer doping [8-11]. Hydrogen terminated diamond is a p-type conductor and induced by electron affinity near the surface [9, 10]. Conductivity is lost by

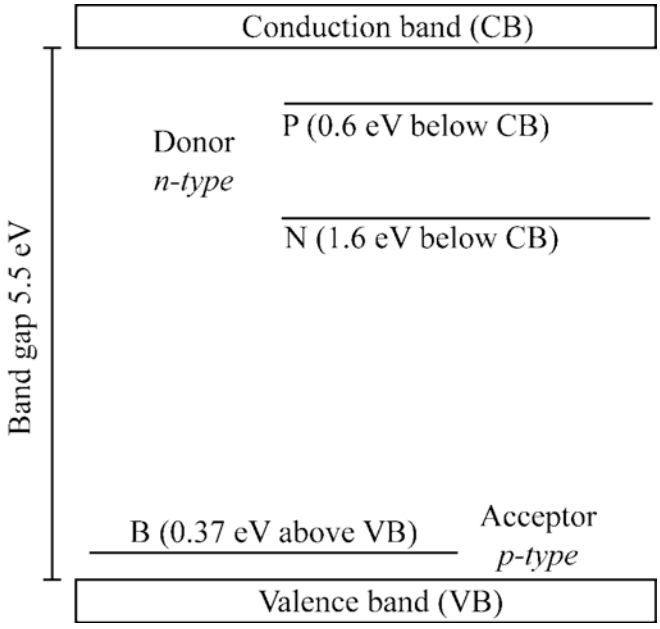

Fig. 1.3. Energy diagrams of selected states in the bandgap of diamond [2, 20].

heat treatment [12, 13] as well as electrochemical processes [14]. For most electrochemical applications, it is necessary to use stable conducting diamond obtained by doping. For this purpose, there are two types of dopants: for *n-type* conductivity, nitrogen (charge carrier activation energy 1.6 - 1.7 eV) [15-17], phosphorus (charge carrier activation energy 0.6 eV) [16, 18, 19], or for *p-type* conductivity, boron (a low charge carrier activation energy 0.37 eV) (**Fig. 1.3**) [3, 20]. Boron-doped diamond (BDD) film has become the most popular material and has been widely studied since the synthesis of *p-type* doping of diamond is much easier than that of *n*-type doping [16].

Diamond, a wide-gap insulator, can be converted to a conductor by boron doping. Conductive boron-doped diamond (BDD) was first grown in 1973 by chemical vapor deposition [21]. The boron-doping agent is usually added by using a fraction of diborane, trimethyl boron or organic borates in the gas phase, while solid-state boron sources have also been used [2, 3]. The conductivity of boron-doped diamond film depends on the doping level. Semi-metallic behavior can be obtained by doping diamond with a high concentration of boron from 10^{18} to 10^{19} cm^{-3} (200-1600 ppm). Good conductivity and electrochemical properties are possible with heavy boron-doping of typically 10^{20} cm^{-3} (2000 ppm) [2], which corresponds to about one boron atom per 1000 carbon atoms.

Boron-doped diamond film is an attractive electrode material for various applications thanks to its wide potential window, dimensional stability and low double layer capacitance compared with other carbonaceous material, which leads to the growth of a new field for fundamental and applied electrochemistry. Various electrochemical applications based on the outstanding properties of BDD electrode have been recognized. Several factors, including primary crystallographic orientation, boron doping level, non-

diamond impurities and surface termination are known to affect its electrochemical properties. Modifications have been proposed for enhancing the intrinsic properties of BDD electrodes, which improves their electrochemical performance for industrial applications.

The small electrochemically active surface area of BDD electrode is disadvantageous for certain electrochemical applications. If the surface area of BDD electrodes can be enhanced without loss of other properties (i.e., conductivity, dimensional stability and wide potential window), it is expected that BDD electrodes can be used for large-scale industrial applications. In particular, porous BDD electrode with large surface area would be advantageous for electrolysis, electro-synthesis and electro-analysis, since higher utilization of diamond surface and operation at higher current density can be realized. Nanostructured BDD has been suggested as an attractive approach [2, 3]. However, the hardness of diamond, consisted of strong covalent sp^3 bonds, makes it difficult to mechanically fabricate porous structures. Preferential etching methods have been adopted to synthesize nanostructured BDD electrodes [2].

1.2. Electrochemical applications of BDD electrodes

Semiconducting diamond electrodes were first used for photo-electrochemistry [23]. The electrochemical applications of boron-doped diamond (BDD) electrodes were reported for the electro-reduction of nitrate to ammonia [24] and analytical applications in 1993 [25]. In recent years, several groups have been heavily involved in the applications of BDD electrodes including Fujishima (Japan) [26-61], Swain (U.S.A.) [62-74], Comninellis (Swiss) [75-97], Pleskov (Russia) [23, 98-101], Angus (U.S.A.) [11, 21, 22, 102-104] as well as Foord and Compton (England) [14, 105-116]. The most interesting properties of BDD electrodes are its superior chemical and dimensional stability, low background current and very wide potential window (**Fig. 1.4**). Many reviews concerning various

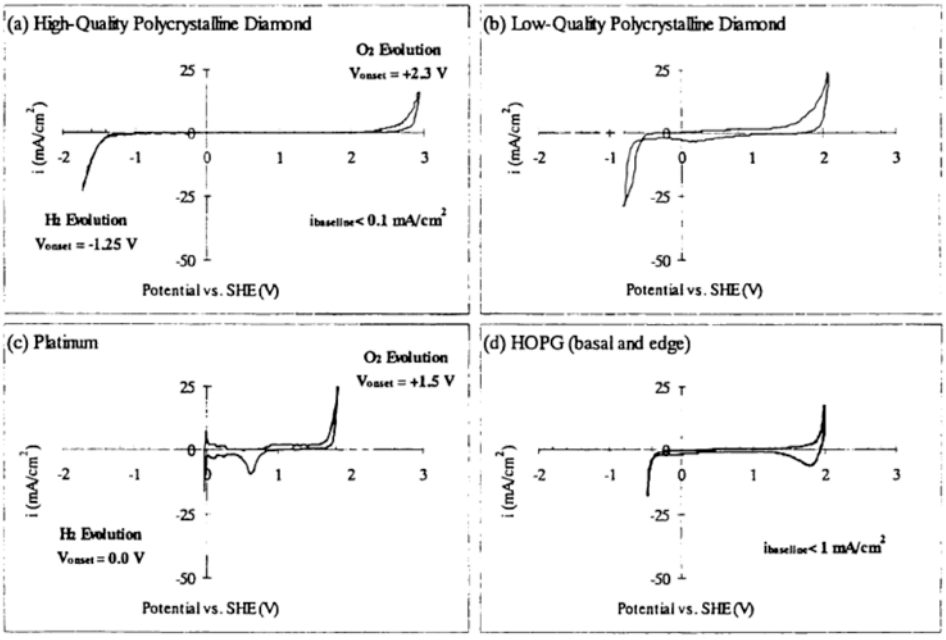

Fig. 1.4. Cyclic voltammograms of various electrodes in 0.5 M H_2SO_4 at scan rate of 200 mV s^{-1}. (a) high-quality diamond, (b) low-quality diamond, (c) platinum, (d) highly ordered pyrolytic graphite [22].

aspects on research and development of BDD electrodes can be found in the literature [20, 30, 98, 99, 117-120]. Here, some representative electrochemical application and properties of BDD electrodes are briefly summarized.

1.2.1. Waste water treatment and water disinfection

Wastewater treatment

Organic compounds in water can be removed through electrochemical reduction and oxidation routes [121, 122]. For reduction processes, some organic pollutants can be converted to nontoxic compounds. For example, halogenated aliphatic compounds can be electrochemically reduced to corresponding dehalogenated aliphatic hydrocarbons (**Equation 1.1**) [2]. In the case of oxidation process, organic pollutants can be oxidized to nontoxic compounds and finally into carbon dioxide (**Equation 1.2**) [3, 75, 121].

$$C_mH_{2m+2-p}Cl_p + 2pe^- + pH^+ \rightarrow C_mH_{2m+2} + pCl^- \quad (1.1)$$

$$C_mH_n + 2mH_2O \rightarrow mCO_2 + (n + 4m)H^+ + (n+4m)e^- \quad (1.2)$$

The weak interaction between the diamond surface and hydroxyl radical leads to a high overpotential for oxygen evolution (wide potential window) and high reactivity for organics oxidation [97]. In general, there are two processes for electrochemical oxidation of organic pollutants by using BDD electrodes, “direct” and “indirect” processes. In the direct processes, organic pollutants in water can be electrochemically oxidized by hydroxyl radicals that are formed by water decomposition [78, 79, 81]. In the indirect processes, the organic pollutants can be oxidized by the generated oxidants (such as O_3, H_2O_2, $H_2S_2O_8$, active chlorine and so on) [80, 81, 86-88, 90, 92, 122, 123].

Water disinfection

Many problems associated with the lack of clean, fresh water are known. In recent years, effective electrochemical disinfection systems for conventional water treatment have been developed, which are based on the electrochemical production of disinfecting agents. The advantages (such as environmentally friendliness, low cost and easy operation) of electrochemical disinfection make them more attractive than other methods (such as physical disinfection) [124-126]. The most popular method of electrochemical disinfection is electrochlorination (such as Cl_2, HClO, ClO^-), generating by using DSA® type anodes based on mixed metal oxides of IrO_2 and/or RuO_2 [124-126]. BDD electrodes show attractive advantages that can be used for electrochemical disinfection. Because of its wide potential window, BDD electrode can further oxidize hypochlorite to chlorate and perchlorate, which are not formed at DSA® type and Pt electrodes [125, 127]. In another case, if water with low or zero chloride concentration is required, the addition of sodium chloride is not acceptable and free chlorine cannot be produced [125]. Therefore, disinfection should be based on other electro-generated species (e.g., ozone). By using BDD electrode as anode, ozone can be produced with much higher current efficiency (up to 47 %) than DSA® type and Pt electrodes [125, 128]. Moreover, BDD thin films deposited on Si, Ti, Nb, and W by chemical vapor deposition also show excellent electrochemical stability that is suited for electrochemical disinfection [3, 117, 121].

1.2.2. Inorganic and organic electro-synthesis

The large overpotential for the evolution of hydrogen and oxygen create a large electrochemical window that should enable a variety of chemical transformations on BDD electrodes. In addition, the remarkable corrosion stability, stability during long-term

cycling in acidic media, and low adsorption properties of BDD electrode are also beneficial to electro-synthesis [117].

Because of the high overpotential for oxygen evolution in aqueous electrolytes, BDD electrodes are suited for the electrochemical production of strongly oxidizing agents. It has been shown for several of these agents that electrochemical production with BDD anodes is superior for the electro-synthesis compared with other electrode materials. Strongly oxidizing inorganic substances can be produced with BDD anodes with higher efficiencies than conventional electrode materials as listed in **Table 1.1**.

Table 1.1. Inorganic substances produced by anodic oxidation with BDD anodes in aqueous electrolyte [20].

E_0 / V vs NHE	Substance	Reaction	Reference
2.20	Ferrate	$Fe^{3+} + 4H_2O \rightarrow FeO_4^{2-} + 3e^- + 8H^+$	32, 130
2.12	Peroxodisulfate	$3HSO_4^- \rightarrow S_2O_8^{2-} + 2H^+ + 2e^-$	83
2.07	Ozone	$3H_2O \rightarrow O_3 + 6e^- + 6H^+$	80, 87, 91, 134
2.07	Peroxodiphosphate	$2PO_4^{3-} \rightarrow P_2O_8^{4-} + 2e^-$	131
1.98	Silver (II)	$Ag^+ \rightarrow Ag^{2+} + e^-$	84
1.80	Peroxycarbonate	$2HCO_3^- \rightarrow C_2O_6^{2-} + 2e^- + 2H^+$	132
1.71	Cerium (IV)	$Ce^{3+} \rightarrow Ce^{4+} + 6e^-$	29
1.60	Periodate	$IO_3^- + H_2O \rightarrow IO_4^- + 2e^- + 2H^+$	133
1.51	Permanganate	$2Mn^{2+} + 4H_2O \rightarrow MnO_4^- + 5e^- + 8H^+$	49

The conversion of organic compounds on BDD electrodes is an emerging field, due to its extremely large potential window in aqueous solutions. They are good substitutes for graphite electrodes because of mechanical, thermal and chemical stability. Some organic reactions, such as alkoxylation [95], fluorination [134] and phenol coupling reactions [135], can be achieved through anodic oxidation on BDD electrode. Some cathodic reactions are also reported by using BDD electrodes, like reduction of oximes and reductive carboxylation [3].

1.2.3. Electroanalytical applications

Electrochemical analysis of biological chemical species with BDD electrode is attractive methods, due to the higher sensitivity, long-term reliability, high accuracy and low cost compared to other detection methods [2]. Glassy carbon and metal electrodes have been typically used for electrochemical detection systems. BDD electrodes are superior to such conventional electrode materials for electroanalysis, due to the wider potential window, higher stability, lower background current and lower adsorption of contaminants [1, 3, 109]. Some substances detected by using BDD electrodes are summarized in **Table 1.2**. Electrochemical detection is sensitive to the pH of electrolyte [44], as well as the surface termination of BDD electrodes. Different surface termination brings about drastic changes in the electrochemical behavior, such as detection of oxalic acid [54]. Oxygen terminated BDD are reported to have better stability in the electroanalysis of chemical species [37].

Table 1.2. Substances detected by using BDD electrodes.

Analyte	Potential / V	pH	Reference
NADH	E_{ox}: 0.58 vs SCE	-	27
Biogenic amines	$E_{1/2}$: 0.9 vs Ag/AgCl	10	66
Biogenic amines	E_{ox}: 0.49 vs SCE	7	33
Caffeine	E_{ox}: 1.8-7.5 vs SCE	1.47-0.19	44
Theophylline	E_{ox}: 1.8-8.9 vs SCE	1.47-0.03	39, 44
Carbamate pesticides	E_{ox}: 1.45 vs Ag/AgCl	7.0	46
Oxalic acid	E_{ox}: 1.32 vs Ag/AgCl	2.1	54
Uric Acid	E_{ox}: 0.76-0.91 vs SCE	1-2.5	37
Chlorophenols	E_{ox}: 1.4 vs SCE	2	39
Azide	E_{ox}: ~1 vs SCE	7.2	64, 67

1.2.4. Electrochemical energy applications

BDD with high mechanical and chemical stability is suggested to be a good support for catalyst, for example as fuel cell catalyst supports. Many efforts have been made to improve adherence and dispersion between the metal and metal oxide particles and BDD surface. Thermal decomposition of appropriate precursors that have been dissolved in suitable solvent is reported to spread metal and metal oxide particles on BDD films. However, the long-term stability is not sufficient at the current state of development [136]. Electro-deposition is another widely used method for the preparation and deposition of metal and metal oxide particles on BDD surface, due to at or near room temperature operation, controlled growth and low cost [136]. In addition, the sol-gel technique is known as a suitable process for coating substrates, because of its advantages, including

better homogeneity, size and morphological control. With the aim to improve electro-catalytic response, the modification of the BDD electrode with Pt-metal oxide catalysts prepared by sol-gel methods has been studied for fuel cell applications [137-140]. The results also indicate that the deposits prepared by sol-gel methods show a good stability on diamond surface [137-140]. Enlarging the surface area of BDD can increase the catalyst loadings, which enhances its performance for fuel cell applications [41].

The use of BDD as an electrode material for electric double layer capacitors has also been studied [36, 38]. Commonly, electrochemical capacitors require electrode materials with not only large surface area but also large overpotential for the evolution of hydrogen and oxygen. The advantage of BDD electrode with a wide potential window in aqueous electrolyte is useful for increasing the cell voltage. In order to enlarge the surface area, honeycomb structured BDD electrodes have been fabricated by oxygen plasma etching with porous alumina masks, which leads to 200-fold increase in surface area [36]. Porous BDD electrode with large surface area and wide potential window in aqueous solution (2.5 V) may be an ideal electrode candidate for electrochemical capacitors.

1.3. Modification of BDD electrodes

The attractive characteristics of BDD electrode have led to innovation in electrochemistry in the past decade. As a way to extend the capabilities of BDD electrode, modifications of BDD surface have attracted much interest. BDD electrodes with functional surfaces and structures may enhance their performance in electrochemistry (such as high capacitance and high catalyst loadings). In this section, several methods of modification will be reviewed.

1.3.1. Electrochemical treatment

The electrochemical behaviors of BDD electrodes are affected by the surface termination. Many redox couples present higher electron transfer kinetics on hydrogen than oxygen terminated BDD [1]. As-produced BDD thin films generally have a hydrogen-terminated surface, which is due to the hydrogen-containing atmosphere during the CVD process [65, 102, 103]. Hydrogen termination is stable for several months when exposed to the atmosphere [65]. However, the surface of BDD is gradually oxidized by oxygen from air, which is detected by using $[Fe(CN)_6]^{3-/4-}$ redox couple on the cathodically pre-treated BDD [141]. As shown in **Fig. 1.5**, the difference in peak potential (ΔE_p) increases with increased exposure time in air, which is associated to a loss of superficial hydrogen due to oxidation by oxygen from air [141]. Thus, the cathodic pre-treatment should be conducted just before electrochemical experiments in order to ensure hydrogen termination [141]. Anodic oxidation has also been widely used as a surface treatment for the electrochemical investigation of BDD electrodes. Carbonyl groups can be introduced on the BDD surface by anodic polarization, which are reactive to DNPH (dinitrophenylhydrazine) [35]. Non-

diamond sp^2-carbon impurities in the BDD film can also be removed during anodic treatment without changes in the crystal shape and size, which leads to a high quality film [39, 47].

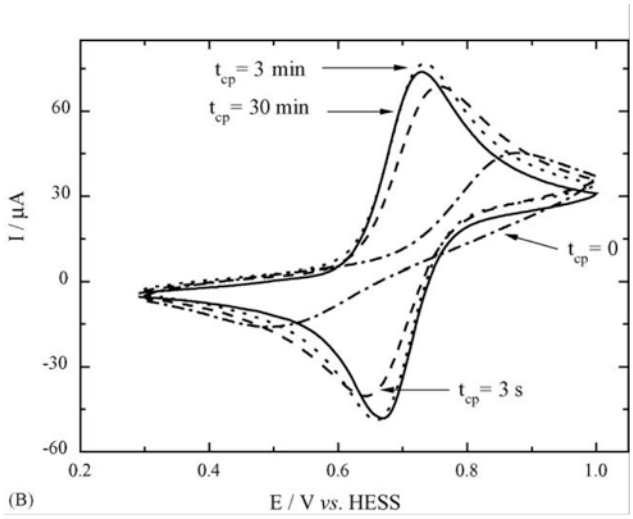

Fig. 1.5. Cyclic voltammograms for catholically pre-treated BDD (800 ppm) recorded in a 1.0 mmol $K_4[Fe(CN)_6]$ + 0.5 mol L^{-1} H_2SO_4 aqueous solution at 0.05 V s^{-1} for different times [141].

1.3.2. Plasma treatment

In order to further functionalize BDD surface, plasma treatments with various gases have been used. It is generally known that BDD electrode surface terminations can be modified by H_2 and O_2 plasma treatments [1, 142]. Plasma treatments with NH_3/N_2 [143], Cl_2 [57], CF_4 [57, 144, 145] and Ar [57] have also been studied to understand the effect of the different surface terminations on the electrochemical behaviors. Short-duration with plasma treatments causes no marked change in surface morphology and crystal quality, while changing the elemental composition, surface wettability and electrochemical properties of diamond surfaces [57, 143]. The electron-transfer kinetics for $[Fe(CN)_6]^{3-/4-}$ and $Fe^{2+/3+}$ at the BDD electrodes decrease after Cl_2 and CF_4 plasma treatments, while the

electron-transfer kinetics for $[Ru(NH_3)_6]^{2+/3+}$ show no change after these plasma treatments [57]. The potential window of fluorinated BDD electrode that is prepared under CF_4-He atmosphere has also been investigated. The result shows an increase in the potential window (5 V in aqueous solution), limited only by the formation of free hydrogen [$E°$ (H• / H_2) −2.3 vs SHE] and [$E°$ (•OH, H^+ / H_2O) 2.74 vs SHE], compared to the 3.5 V of H-terminated BDD electrodes [144].

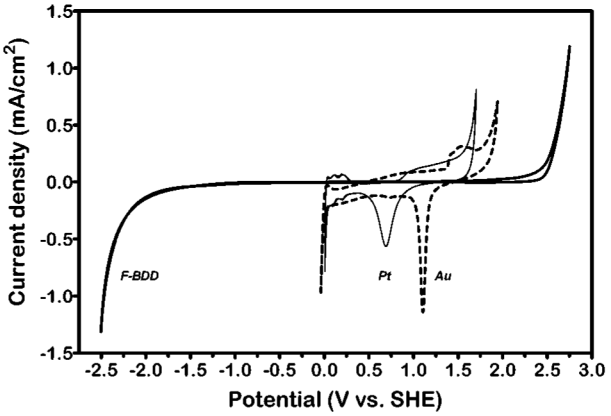

Fig. 1.6. Cyclic voltammograms of fluorinated BDD, platinum and gold electrodes in 1 M $HClO_4$ at scan rate of 0.2 V s^{-1} [144].

1.3.3. Etching of BDD electrodes

Various etching methods have been adopted to modify BDD surface. Highly ordered honeycomb structures on BDD surface are fabricated by oxygen plasma etching through an alumina mask (**Fig. 1.7**(a and a')) [36, 38]. The BDD honeycomb exhibits 200 times higher capacitance than that of as-deposited BDD with the same wide electrochemical potential window (2.5 V) [36]. Oxygen plasma etching without mask fabricates a whisker structure on the highly boron-doped diamond substrates (**Fig. 1.7**(b)), and the effect of the etching conditions and the boron concentration in diamond on the whisker morphology is

investigated [61]. Vertically aligned BDD nanowires with controlled length of wires and distance between wires are fabricated by reactive ion etching with nanodiamond particles as a hard mask (**Fig. 1.7**(c)) [146, 147]. Due to advantages such as chemical stability, low background current and hardness forming a robust biosensing interface, BDD nanowire is applied for electrochemical DNA detection, resulting in high sensitivity as well as in single-base mismatch discrimination [146, 147]. Nano-porous structure can be formed on BDD surface through catalytic (Ni) etching in a hydrogen atmosphere (**Fig. 1.7**(b, b' and b'')) [148]. The etching method is an effective way for fabricating nanostructured BDD electrodes, which can enhance its electrochemical performance for practical applications.

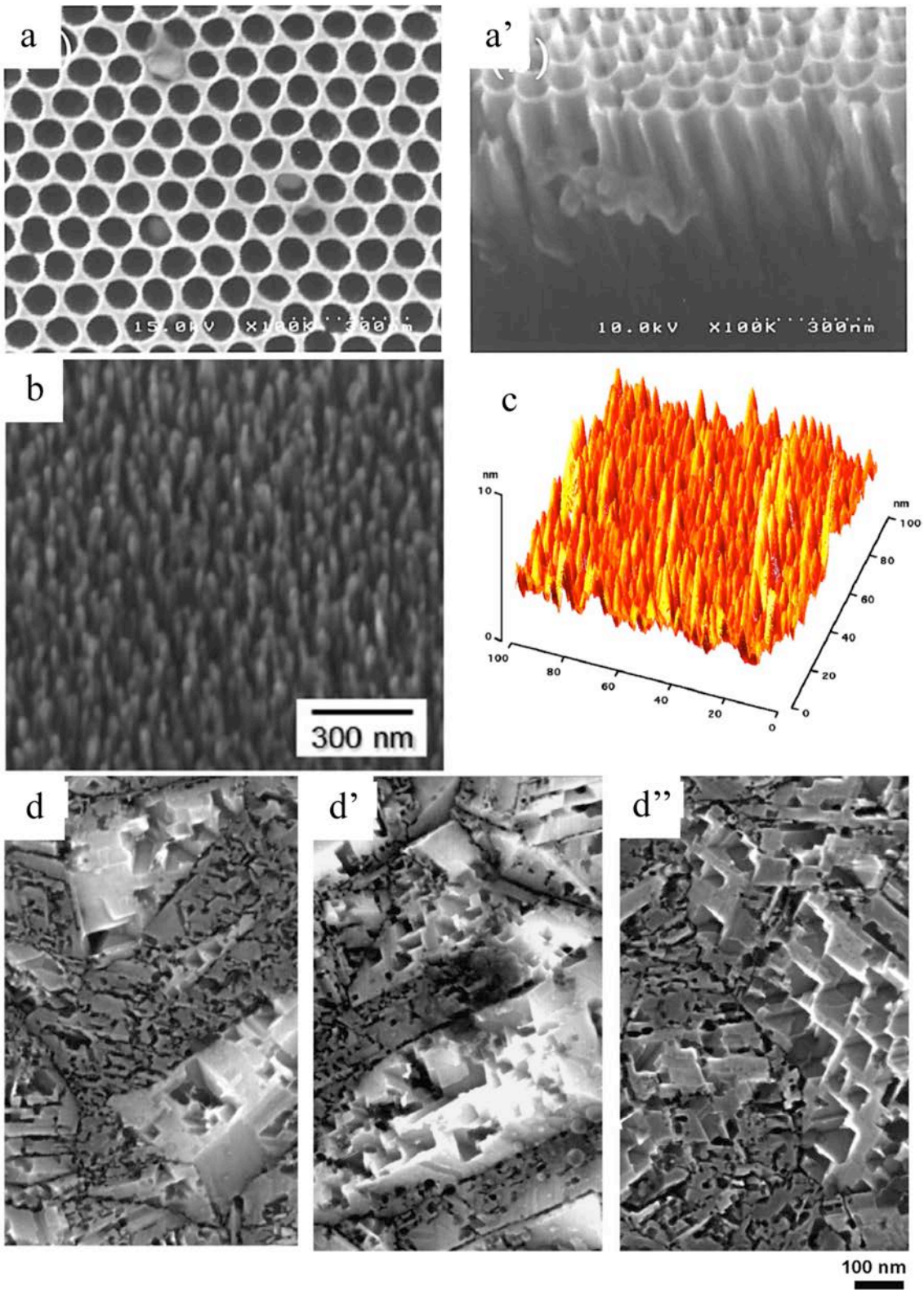

Fig. 1.7. SEM images of (a and a') nanoporous honeycomb BDD fabricated by oxygen plasma etching with alumina mask [36, 38], (b) BDD whisker fabricated by maskless oxygen plasma etching [61], (c) BDD nanowires fabricated by reactive ion etching with nanodiamond particles as a hard mask [146, 147], (d) nano-porous BDD fabricated with Ni as catalysts through heat treatment in a flowing gas mixture of H_2 (10 %) and N_2 (90 %) at 900 °C for (d) 2 h, (d') 10 h and (d'') 24 h [148].

1.4. Objective of this thesis

Conductive boron-doped diamond (BDD) is a novel electrode material for various electrochemical applications owing to its wide potential window, electrochemical stability and low background current compared to other carbonaceous materials. Fabrication of nanostructures on BDD surfaces without loss of other properties (i.e., conductivity, dimensional stability, wide potential window) may enhance the performance for specific application. The objective of this thesis is to study steam and CO_2 activation with emphasis on the fundamental mechanism of preferential etching for boron-doped polycrystalline diamond electrodes. The effect of boron content on steam activation of BDD was studied by using BDD with different boron content (800, 2500 and 5000 ppm boron) (Chapter 2). In chapter 3, CO_2 activation was conducted on polycrystalline BDD electrode (800 ppm) composed of a mixture of {111} and {100} planes for investigating the etching behavior.

References

[1] F. P. Bundy, H. T. Hall, H. M. Strong and R. H. Wentorf, *Nature*, **176**, 55 (1955).

[2] A. Fujishima, Y. Einaga, T. N. Rao and D. A. Tryk, Diamond Electrochemistry, Elsevier Amsterdam-BKC, Tokyo, 2005.

[3] E. Brillas and C. A. Martínez Huitle, Synthetic Diamond Films: Preparation, Electrochemistry, Characterization and Applications, John Wiley & Sons, Hoboken, NJ, USA, 2011.

[4] K. Nassau and J. Nassau, *J. Cryst. Grwot.*, **46**, 172 (1979).

[5] S. Matsumoto, Y. Sato, M. Tsutsumi and N. Setaka, *J. Mater. Sci.*, **17**, 3106 (1982).

[6] P. K. Bachmann and R. Messier, *Chem. Eng. News*, **67**, 24 (1989).

[7] I. M. Landstrass and K. V. Ravi, *Appl. Phys. Lett.*, **55**, 975 (1989).

[8] F. Maier, M. Riedel, B. Mantel, J. Ristein and L. Ley, *Phys. Rev. Lett.*, **85**, 3472 (2000).

[9] J. Ristein, M. Riedel and L. Ley, *J. Electrochem. Soc.*, **151**, E315 (2004).

[10] J. Ristein, *Appl. Phys. A*, **82**, 377 (2006).

[11] V. Chakrapani, S. C. Eaton, A. B. Anderson, M. Tabib-Azar and J. C. Angus, *Electrochem. Solid-State Lett.*, **8**, E4 (2005).

[12] R. Ramesham, T. Roppel, C. Ellis and B. H. Loo, *J. Electrochem. Soc.*, **138**, 2981 (1991).

[13] R. Ramesham, M. F. Rose, R. F. Askew, T. L. Bekker, J. A. Dayton, I. L. Krainsky, G. Mearini, D. Filed, A. S. Gilmour and V. Ayres, *Surf. Coat. Tech.*, **64**, 81 (1994).

[14] A. Chatterjee, R. G. Compton, J. S. Foord, M. Hiramatsu and F. Marken, *Phys. Stat. Sol. (a)*, **199**, 49 (2003).

[15] R. Kalish, *Carbon*, **37**, 781 (1999).

[16] R. Kalish, *Diamond Relat. Mater.*, **10**, 1749 (2001).

[17] Q. Chen, D. M. Gruen, A. R. Krauss, T. D. Corrigan, M. Witek and G. M. Swain, *J. Electrochem. Soc.*, **148**, E44 (2001).

[18] M. Neladek, *Semicond. Sci. Technol.*, **20**, R19 (2005).

[19] S. Koizumi and M. Suzuki, *Phys. Stat. Sol. (a)*, **203**, 3358 (2006).

[20] A. Kraft, *Int. J. Electrochem. Sci.*, **2**, 355 (2007).

[21] D. J. Poferl, N. C. Gardner and J. C. Angus, *J. Appl. Phys.*, **44**, 1428 (1973).

[22] J. C. Angus, H. B. Martin, U. Landau, Y. E. Estefeeva, B. Miller and N. Vinokur, *New Diamond Front. Carbon Technol.*, **9**, 175 (1999).

[23] Yu. V. Pleskov, A. Ya. Sakharova, M. Krotova, L. L. Bouilov and B. V. Spitsyn, *J. Electroanal. Chem.*, **228**, 19 (1987).

[24] R. Tanne, K. Patel, K. Hashimoto and A. Fujishima, *J. Electroanal. Chem.*, **347**, 409 (1993).

[25] G. M. Swain and R. Ramesham, *Anal. Chem.*, **65**, 345 (1993).

[26] A. Fujishima, T. N. Rao, E. Popa, B. V. Sarada, I. Yagi and D. A. Tryk, *J. Electroanal. Chem.*, **473**, 179 (1999).

[27] T. N. Rao, I. Yagi, T. Miwa, D. A. Tryk and A. Fujishima, *Anal. Chem.*, **71**, 2505 (1999).

[28] B. V. Sarada, T. N. Rao and D. A. Tryk, *J. Electrochem. Soc.*, **146**, 1469 (1999).

[29] Y. Maeda, K. Sato, R. Ramaraj, T. N. Rao, D. A. Tryk and A. Fujishima, *Electrochim. Acta*, **44**, 3441 (1999).

[30] T. N. Rao and A. Fujishima, *Diamond Relat. Mater.*, **9**, 384 (2000).

[31] H. Masuda, M. Watanabe, K. Yasui, D. A. Tryk, T. N. Rao and A. Fujishima, *Adv. Mater.*, **12**, 444 (2000).

[32] J. Lee, D. A. Tryk, A. Fujishima and S. M. Park, *Chem. Comm.*, **486**, (2000).

[33] B. V. Sarada, T. N. Rao, D. A. Tryk and A. Fujishima, *Anal. Chem.*, **72**, 1632 (2000).

[34] T. N. Rao, B. V. Sarada, D. A. Tryk and A. Fujishima, *J. Electroanal. Chem.*, **491**, 195 (2000).

[35] H. Notsu, I. Yagi, T. Tatsuma, D. A. Tryk and A. Fujishima, *J. Electroanal. Chem.*, **492**, 31 (2000).

[36] K. Honda, T. N. Rao, D. A. Tryk, A. Fujishima, M. Watanabe, K. Yasui and H. Masuda, *J. Electrochem. Soc.*, **147**, 659 (2000).

[37] E. Popa, Y. Kubota, D. A. Tryk and A. Fujishima, *Anal. Chem.*, **72**, 1724 (2000).

[38] K. Honda, T. N. Rao, D. A. Tryk, A. Fujishima, M. Watanabe, K. Yasui, and H. Masuda, *J. Electrochem. Soc.*, **148**, A668 (2001).

[39] A. Fujishima and T. N. Rao, *Diamond Relat. Mater.*, **10**, 1799 (2001).

[40] N. Spataru, B. V. Sarada, E. Popa, D. A. Tryk and A. Fujishima, *Anal. Chem.*, **73**, 514 (2001).

[41] K. Honda, M. Yoshimura, Tata N. Rao, D. A. Tryk, A. Fujishima, K. Yasui, Y. Sakamoto, K. Nishio and H. Masuda, *J. Electroanal. Chem.*, **514**, 35 (2001).

[42] D. Shin, B. V. Sarada and D. A. Tryk, *Chem. Sens.*, **18**, 124 (2002).

[43] N. Spataru, B. V. Sarada, D. A. Tryk and A. Fujishima, *Electroanal*., **14**, 721 (2002).

[44] S. Okuyama, S. I. Matsushita and A. Fujishima, *Langmuir*, **18**, 8282 (2002).

[45] T. N. Rao, B. H. Loo, B. V. Sarada, C. Terashima and A. Fujishima, *Anal. Chem.*, **74**, 1578 (2002).

[46] C. Terashima, T. N. Rao, B. V. Sarada, D. A. Tryk and A. Fujishima, *Anal. Chem.*, **74**, 895 (2002).

[47] I. Duo, C. Levy-clement, A. Fujishima and C. Comninellis, *J. Appl. Electrochem.*, **34**, 935 (2004).

[48] K. Honda, M. Yoshimura, K. Kawakita, A. Fujishima, Y. Sakamoto, K. Yasui, N. Nishio and H. Masuda, *J. Electrochem. Soc.*, **151**, A532 (2004).

[49] J. Lee, Y. Einaga, A. Fujishima and S. M. Park, *J. Electrochem. Soc.*, **151**, E265 (2004).

[50] T. A. Ivandini, R. Sato, Y. Makide, A. Fujishima and Y. Einaga, *Diamond Relat. Mater.*, **13**, 2003 (2004).

[51] K. Kondo, K. Honda, D. A. Tryk and A. Fujishima, *J. Electrochem. Soc.*, **152**, E18 (2005).

[52] T. A. Ivandini, R. Sato, Y. Makide, A. Fujishima and Y. Einaga, *Diamond Relat. Mater.*, **14**, 2133 (2005).

[53] K. Arihara, C. Terashima and A. Fujishima, *Electrochem. Solid State Lett.*, **9**, D17 (2006).

[54] T. A. Ivandini, R. Sato, Y. Makide, A. Fujishima and Y. Einaga, *Anal. Chem.*, **78**, 6291 (2006).

[55] T. Ochiai, K. Arihara, C. Terashima and A. Fujishima, *Chem. Lett.*, **35**, 1018 (2006).

[56] T. A. Ivandini, T. N. Rao, A. Fujishima and Y. Einaga, *Anal. Chem.*, **78**, 3467 (2006).

[57] T. Kondo, H. Ito, K. Kusakabe, K. Ohkawa, Y. Einaga, A. Fujishima and T. Kawai, *Electrochim. Acta*, **52**, 3841 (2007).

[58] T. A. Ivandini, K. Honda, T. N. Rao, A. Fujishima and Y. Einaga, *Talanta*, **71**, 648

(2007).

[59] A. Suzuki, T. A. Ivandini, A. Kamiya, S. Nomura, M. Yamanuki, K. Matsumoto, A. Fujishima and Y. Einaga, *Sens. Actuat. B*, **120**, 500 (2007).

[60] M. Wei, C. Terashima, M. Lv, A. Fujishima and Z. Z. Gu, *Chem. Comm.*, 3624 (2009).

[61] C. Terashima, K. Arihara, S. Okazaki, T. Shichi, D. A. Tryk, T. Shirafuji, N. Saito, Osamu Takai and A. Fujishima, *Appl. Mater. Interfaces*, **3**, 177 (2011).

[62] J. W. Strojek, M. C. Granger, G. M. Swain, T. Dallas and M. W. Holtz, *Anal. Chem.*, **68**, 2031 (1996).

[63] S. Jolley, M. Koppang, T. Jackson and G. M. Swain, *Anal. Chem.*, **69**, 4099 (1997).

[64] J. Xu and G. M. Swain, *Anal. Chem.*, **70**, 1502 (1998).

[65] G. M. Swain, A. B. Anderson and J. C. Angus, *MRS Bulletin*, **23**, 56 (1998).

[66] M. D. Koppang, M. Witek, J. Blau and G. M. Swain, *Anal. Chem.*, **71**, 1188 (1999).

[67] M. C. Granger, J. Xu, J. W. Strojek and G. M. Swain, *Anal. Chim. Acta*, **397**, 145 (1999).

[68] M. A. Witek and G. M. Swain, *Anal. Chim. Acta*, **440**, 119 (2001).

[69] P. Sonthalia, E. McGaw, Y. Show and G. M. Swain, *Anal. Chim. Acta*, **522**, 32 (2004).

[70] J. A. Bennett, J. Wang, Y. Show and G. M. Swain, *J. Electrochem. Soc.*, **151**, E306 (2004).

[71] J. Park, Y. Show, V. Quaiserova, K. Peckova, J. J. Galligan, G. D. Fink and G. M. Swain, *J. Electroanal. Chem.*, **583**, 56 (2005).

[72] A. E. Fischer and G. M. Swain, *J. Electrochem. Soc.*, **152**, B359 (2005).

[73] E. A. McGaw and G. M. Swain, *Anal. Chim. Acta*, **575**, 180 (2006).

[74] M. C. Granger, J. Xu, J. W. Strojek and G. M. Swain, *Anal. Chim. Acta*, **397**, 145 (2006).

[75] C. Comninellis, *Electrochim. Acta*, **39**, 1857 (1994).

[76] O. Simond, V. Schaller and C. Comninellis, *Electrochim. Acta*, **42**, 2009 (1997).

[77] O. Simond and C. Comninellis, *Electrochim. Acta*, **42**, 2013 (1997).

[78] M. Fryda, D. Herrmann, L. Schafer, C. P. Klages, A. Perret, W. Haenni, C. Comninellis and D. Gandini, *New Diamond Front. Carbon Technol.*, **9**, 229 (1999).

[79] A. Perret, W. Haenni, N. Skinner, T. M. Tang, D. Gandini, C. Comninellis, B. Correa, and G. Foti, *Diamond. Relat. Mater.*, **8**, 820 (1999).

[80] G. Foti, D. Gandini, Ch. Comninellis, A. Perret and W. Haenni, *Electrochem. Solid State Lett.*, **2**, 228 (1999).

[81] D. Gandini, E. Mahe, P. A. Michaud, W. Haenni, A. Perret and C. Comninellis, *J. Appl. Electrochem.*, **30**, 1345 (2000).

[82] S. Ferro, A. De Battisti, I. Duo, C. Comninellis, W. Haenni and A. Perret, *J. Electrochem. Soc.*, **147**, 2614 (2000).

[83] P. A. Michaud, E. Mahe, W. Haenni, A. Perret and C. Comninellis, *Electrochem. Solid State Lett.*, **3**, 77 (2000).

[84] M. Panizza, I. Duo, P. A. Michaud, G. Cerisola and C. Comninellis, *Electrochem. Solid-State Lett.*, **3**, 550 (2000).

[85] J. Iniesta, P. A. Michaud, M. Panizza, G. Cerisola, A. Aldaz and C. Comninellis, *Electrochim. Acta*, **46** (23), 3573 (2001).

[86] M. Panizza, P. A. Michaud, G. Cerisola and C. Comninellis, *J. Electroanal. Chem.*, **507**, 206 (2001).

[87] J. Iniesta, P. A. Michaud, M. Panizza and Ch. Comninellis, *Electrochem. Commun.*, **3**, 346 (2001).

[88] M. A. Rodrigo, P. A. Michaud, I. Duo, M. Panizza, G. Cerisola and Ch. Comninellis, *J. Electrochem. Soc.*, **148**, D60 (2001).

[89] W. Haenni, J. Gobet, L. Pupunat. P. Rychen, C. Comninellis and B. Correa, *New Diamond Front. Carbon Technol.*, **12**, 83 (2002).

[90] F. Montilla, P. A. Michaud, E. Morallon, J. L. Vazquez and C. Comninellis, *Electrochim. Acta*, **47**, 3509 (2002).

[91] P. A. Michaud, M. Panizza, L. Ouattara, T. Diaco, G. Foti and C. Comninellis, *J. Appl. Electrochem.*, **33**, 151 (2003).

[92] B. Marselli, J. Garcia-Gomez, P. A. Michaud, M. A. Rodrigo and Ch. Comninellis, *J. Electrochem. Soc.*, **150**, D79 (2003).

[93] B. E. Roustom, G. Foti and Ch. Comninellis, *Electrochem. Commun.*, **7**, 398 (2005).

[94] E. Mahe, D. Devilliers and C. Comninellis, *Electrochim. Acta*, **50**, 2263 (2005).

[95] R. Fardel, U. Griesbach, H. Putter and C. Comninellis, *J. Appl, Electrochem.*, **36**, 249 (2006).

[96] G. Sine, L. Ouattara, M. Panizza and C. Comninellis, *Electrochem. Solid State Lett.*, **6**, D9 (2006).

[97] A. Kapalka, G. Foti and C. Comninellis, *J. Appl. Electrochem.*, **38**, 7 (2008).

[98] Yu. V. Pleskov, *Russ. Chem. Rev.*, **68**, 381 (1999).

[99] Yu. V. Pleskov, *Russ. J. Electrochem.*, **38**, 1275 (2002).

[100] Yu. V. Pleskov, Yu. E. Evstefeeva, V. P. Varnin, and I. G. Teremetskaya, *Russ. J. Electrochem.*, **40**, 1023 (2004).

[101] Yu. V. Pleskov, Yu. E. Evstefeeva, M. D. Krotova, V. P. Varnin and I. G. Teremetskaya, *J. Electroanal. Chem.*, **595**, 168 (2006).

[102] H. B. Martin, A. Argoitia, J. C. Angus and U. Landau, *J. Electrochem. Soc.*, **146**, 2959 (1996).

[103] H. B. Martin, A. Argoitia, U. Landau, A. B. Anderson and J. C. Angus, *J. Electrochem. Soc.*, **143**, 133 (1996).

[104] L. F. Li, D. A. Totir, B. Miller, G. Chottiner, A. Argoitia, J. C. Angus and D. A. Scherson, *J. Am. Chem. Soc.*, **119**, 7875 (1997).

[105] A. J. Saterlay, J. S. Foord and R. G. Compton, *Analyst*, **124**, 1791 (1999).

[106] A. J. Saterlay, D. F. Tibbetts and R. G. Compton, *Anal. Sci.*, **16**, 1055 (2000).

[107] A. Chatterjee, R. Wiltshire, K. B. Holt, R. G. Compton, J. S. Foord and F. Marken, *Diamond Relat. Mater.*, **11**, 646 (2002).

[108] C. Prado, G. U. Flechsig, P. Gründler, J. S. Foord, F. Marken and R. G. Compton, *Analyst*, **127**, 3 (2002).

[109] R. G. Compton, J. S. Foord and F. Marken, *Electroanal.*, **15**, 1349 (2003).

[110] K. B. Holt, C. Forryan, R. G. Compton, J. S. Foord and F. Marken, *New J. Chem.*, **27**, 698 (2003).

[111] C. Prado, S. J. Wilkins, P. Gründler, F. Marken and R. G. Compton, *Electroanal.*, **15**, 1011 (2003).

[112] J. S. Foord, K. Eaton, W. Hao and A. Crossley, *Phys. Chem. Chem. Phys.*, **7**, 2787 (2005).

[113] J. S. Foord and A. S. Chatterjee, *Phys. Stat. Sol. A*, **202**, 2110 (2005).

[114] C. M. Welch, M. E. Hyde, C. E. Banks and R. G. Compton, *Anal. Sci.*, **21**, 1421 (2005).

[115] N. S. Lawrence, M. Pagels, A. Meredith, T. G. J. Jones, C. E. Hall, C. S. J. Pickles, H. P. Godfried, C. E. Banks, R. G. Compton and L. Jiang, *Talanta*, **69**, 829 (2006).

[116] C. E. Banks, M. E. Hyde, P. Tomcik, R. Jacobs and R. G. Compton, *Talanta*, **62**, 279 (2007).

[117] M. Panizza and G. Cerisola, *Electrochim. Acta*, **51**, 191 (2005).

[118] Y. Shao, J. Liu, Y. Wang and Y. Lin, *J. Mater. Chem.*, **19**, 46 (2009).

[119] J. H. T. Luong, K. B. Male and J. D. Glennon, *Analyst*, **134**, 1965 (2009).

[120] K. E. Toghill and R. G. Compton, *Electroanal.*, **22**. 1947 (2010).

[121] C. A. Martinez-Huitle and S. Ferro, *Chem. Soc. Rev.*, **35**, 1324 (2006).

[122] P. Canizares, C. Saez, J. Lobato and M. A. Rodrigo, *Electrochim. Acta*, **49**, 4641 (2004).

[123] P. Canizares, J. Garcia-Gomez, J. Lobato and M. A. Rodrigo, *Ind. Eng. Chem. Res.*, **43**, 1915 (2004).

[124] C. A. Martinez-Huitle and E. Brillas, *Angew Chem. Int. Ed.*, **47**, 1998 (2008).

[125] A. Kraft, *Platinum Metals Rev.*, **52**, 177 (2008)

[126] M. I. Kerwick, S. M. Reddy, A. H. L. Chamberlain and D. M. Holt, *Electrochim. Acta*, 50, 5270 (2008).

[127] S. Palmas, A. M. Polcaro, A. Vacca, M. Mascia and F. Ferrara, *J. Appl. Electrochem.*, **37**, 1357 (2007).

[128] A. Kraft, M. Stadelmann and M. Wunsche, *Electrochem. Commun.*, **8**, 883 (2006).

[129] P. Canizares, M. Arcis, C. Saez and M. A. Rodrigo, *Electrochem. Commun.*, **9**, 2286 (2007).

[130] N. Katsuki, E. Takahashi, M. Toyoda, T. Kurosu, M. Iida, S. Wakita, Y. Nishiki and T. Shimamume, *J. Electrochem. Soc.*, **145**, 2358 (1998).

[131] P. Canizares, F. Larrondo, J. Lobat, M. A. Rodrigo and C. Saez, *J. Electrochem. Soc.*, **152**, D191 (2005).

[132] M. S. Saha, T. Furuta and Y. Nishiki, *Electrochem. Solid State Lett.*, **6**, D5 (2003).

[133] L. J. J. Janssen and M. H. A. Bljilevens, *Electrochim. Acta*, **48**, 3959 (2003).

[134] F. Okino, H. Shibata, S. Kawasaki, H. Touhara, K. Momota, M. Nishitani-Gamo, I. Sakaguchi and T. Ando, *Electrochem. Solid State Lett.*, **2**, 382 (1999).

[135] A. Kirste, G. Schnakenburg, F. Stecker, A. Fischer and S. R. Waldvogel, *Angew. Chem. Int. Ed.*, **49**, 971 (2010).

[136] K. I. B. Eguiluz, J. M. Peralta-Hernández, A. Hernández-Ramírez, J. L. Guzmán-Mar, L. Hinojosa-Reyes, C. A. Martínez-Huitle and G. R. Salazar-Banda, *Int. J. Electrochem.*, **2012**, 1 (2012).

[137] H. B. Suffredini, V. Tricoli, L. A. Avaca, and N. Vatistas, *Electrochem. Commun.*, **6**, 1025 (2004).

[138] G. R. Salazar-Banda, H. B. Suffredini, M. L. Calegaro, S. T. Tanimoto and L. A. Avaca, *J. Power Sources*, **162**, 9 (2006).

[139] H. B. Suffredini, V. Tricoli, N. Vatistas and L. A. Avaca, *J. Power Sources*, **158**, 124 (2006).

[140] G. R. Salazar-Banda, H. B. Suffredini, L. A. Avaca and S. A. S. Machado, *Mater. Chem. Phys.*, **117**, 434 (2009).

[141] G. R. Salazar-Banda, L. S. Andrade, P. A. P. Nascente, P. S. Pizani, R. C. Rocha-Filho and L. A. Avaca, *Electrochim. Acta*, **51**, 4612 (2006).

[142] N. Simon, D. Ballutaud, M. Herlem and A. Etcheberry, *Diamond Relat. Mater.*, **13**, 1050 (2004).

[143] N. Simon, C. Decorse-Pascanut, A. M. Gonçalves, D. Ballutaud, G. Charrier and A. Etcheberry, *Diamond Relat. Mater.*, **18**, 890 (2009).

[144] S. Ferro and A. De Battisti, *Anal. Chem.*, **75**, 7040 (2003).

[145] A. Denisenko, A. Romanyuk, C. Pietzka, J. Scharpf and E. Kohn, *Diamond Relat. Mater.*, **19**, 423 (2010).

[146] N. Yang, H. Uetsuka, E. Osawa, and C. E. Nebel, *Angew. Chem. Int. Ed.*, **47**, 5183 (2008).

[147] N. Yang, H. Uetsuka, E. Osawa and C. E. Nebel, *Nano Lett.*, **8**, 3572 (2008).

[148] T. Ohashi, W. Sugimoto and Y. Takasu, *Electrochim. Acta*, **54**, 5223 (2009).

Chapter 2

Effect of the boron content on the steam activation of boron-doped diamond electrodes

2.1. Introduction

BDD electrodes have been applied to electrochemical wastewater treatment [1-4] as well as electrolytic production of ozone [2, 5] and NF_3 [6]. However, the small electrochemically active surface area is disadvantageous for industrial applications, as large-scale electrodes are necessary. The development of high-surface area of BDD electrodes while maintaining other distinctive properties (i.e., conductivity, dimensional stability, wide potential window) is desired. Three methods have so far been developed for the preparation of porous BDD electrodes; namely dry etching, catalytic etching and steam activation. Dry etching of BDD with oxygen plasma through porous alumina masks gives honeycomb structures with 30−400 nm diameter cylindrical pores [7]. Nanoscale pits and channels can be prepared by catalytic etching of BDD with hydrogen gas using metal nanoparticles as catalysts [8, 9]. Steam activation, which is usually operated at 800-1000 °C and atmospheric pressure, is a conventional manufacturing process of activated carbon [10-16]. We have reported that steam activation leads to roughening of the BDD surface with a distinctive columnar texture [17]. Another characteristic of steam activation is that graphitic impurities are removed during the activation process, affording a wider potential window than the pristine BDD.

Diamond etching by gas phase (O_2 and H_2O) has been studied for fundamental understanding the etching behavior on different diamond planes. The etching experiments on natural diamond planes at 800 or 1400 °C in air revealed a number of different pit morphologies on the {111}, {110} and {100} planes [18]. Etching of diamond {111} and {100} planes at a temperature range of 700-900 °C by dry O_2 and O_2/H_2O were also investigated [19-21]. The results show that {111} surface is completely rough without any

crystallographic orientation, while etched {100} surface are covered with numerous small and shallow pits as well as large and steeper pits. The different etching behavior on diamond is explained by the different reactions between the diamond surfaces and the adsorbed oxygen [19-21]. Theoretical studies by using thermal and hyperthermal oxygen atomic indicates that the diamond {100} planes are more resistant to erosion than {111} planes [22-24]. The study of diamond oxidation by H_2O fluids at high temperature and high pressure (1150-1500 °C and 1 GPa) shows different etching degree between {111} and {100} plane, indicating that the relative oxidation rate is sensitive to diamond plane [25]. In a previous work [17], steam activation was conducted on BDD electrodes with a fixed boron content of 1300 ppm at different activation temperatures (700, 800 and 900 °C) with emphasis on the progressive etching behavior. High temperature activation leads to a porous surface with a characteristic columnar microstructure. The characteristic etching behavior was suggested to be a result of the preferential etching of the {111} plane based on microstructural observation of the etched surface. In order to understand the details of the possible preferential etching, in particular the initial stages of the activation process, this chapter reports the steam activation of BDD electrodes with different levels of boron doping (800, 2500 and 5000 ppm boron) at 800 °C. It is known that the boron-doping level affects the crystal morphology of polycrystalline BDD electrode with the fraction of {111} planes increasing as the B/C ratio increases [26].

2.2. Experimental Section

Boron-doped were synthesized by hot filament-assisted chemical vapor deposition on Nb substrate (2 × 2 cm^2). BDD with boron content of 800, 2500 and 5000 ppm was prepared, and will be denoted as BDD(800), BDD(2500) and BDD(5000), respectively. The BDD electrodes were positioned in a silica boat with the BDD facing up and set in a silica furnace tube. Steam activation was conducted in the following manner. Ultrapure water (>18 MΩ cm) was introduced at saturated vapor pressure (40 °C) into the silica furnace tube at 100 mL min^{-1} with N_2 (99.99995 %) as the carrier gas. The furnace temperature was raised to 800 °C at a rate of 5 °C min^{-1} and held for 2 h. Activation process was conducted in an open system with the outlet gas exposed to atmospheric pressure. The electrodes after steam activation will be denoted as a-BDD(800), a-BDD(2500) and a-BDD(5000). Steam activation of non-doped diamond films were conducted in the same manner for BDD electrodes.

The etching of pure diamond by steam activation was conducted using diamond crystallites with an average diameter of 0.3 mm (TOMEI DIAMOND Co. Ltd., IMS-25), following the method for diamond film. The diamond crystallites have a cubo-octahedral structure with well-defined {111} and {100} planes.

A field emission-scanning electron microscope (FE-SEM; Hitachi S-5000) was used for morphological observation. Atomic force microscopy (Bruker, Digital Instruments Nanoscope III ADC 5) was performed in air using silicon cantilevers (Bruker, NCHV-A) and a 130 μm scanner (AS-130V). The crystalline structure of the pristine BDD was characterized by X-ray diffraction (XRD, Rigaku RINT-2500HF/PC with monochromated CuKα radiation at 40 kV and 40 mA). The microstructure was characterized by Raman

spectroscopy (Kaiser Optical Systems, Inc., Raman Microscope System 3000) with a YAG laser (excitation wavelength 532 nm) as the excitation source. X-ray photoelectron spectroscopy (XPS) was performed on a Kratos Axis Ultra DLD X-ray photoelectron spectrometer with a standard Mg Kα (1256.6 eV) X-ray source operated at 15 mA and 15 kV. All binding energies were referenced to Au ($4f_{7/2}$) at 83.7 eV. The C1s spectra were fitted with asymmetric mixed Gaussian-Lorentzian sum functions using the XPS peak fitting software XPSpeak (version 4.1).

Electrochemical measurements were performed in a single compartment glass cell (Princeton Applied Research, Model K0235 Flat Cell) with a potentio/galvanostat (ALS/CH Instruments; Model 760). A Ag/AgCl (sat. KCl) electrode (0.2223 V *vs*. RHE) was used as the reference electrode and a platinum mesh served as the counter electrode. The exposed geometric area of the working electrode was 1 cm^2. A Luggin capillary was positioned facing the working electrode at a distance of 1 mm. All measurements were performed at 25 ± 1 °C in 0.5 M H_2SO_4 de-aerated by nitrogen gas.

2.3. Results and discussion

As a preliminary control experiment, non-doped diamond crystallites were subjected to steam activation in order to gain a macroscopic insight into the activation process. Typical FE-SEM images of diamond particles after steam activation at 900 °C for 2 h are shown in **Fig. 2.1**. After steam activation, the {100} plane (**Fig. 2.1**(a')) has point-bottomed square shaped pits with large size of 0.5 - 2 μm and pit density of 0.8 pits μm^{-2}. The {111} plane is heavily etched with 0.5 - 3 μm sized triangular pits with pit density of 0.13 pits μm^{-2} (**Fig. 2.1**(b')). Many steps can be observed on the walls of the triangular pits on the steam-activated {111} plane. The surface roughness (*R*) was obtained from AFM images (**Fig. 2.2**). Before activation, the roughness is $R < 10$ nm for both {100} and {111} planes. The roughness of the steam-activated {111} plane is $R = 169$ nm, approximately two times higher than steam-activated {100} plane ($R = 89$ nm). Steam activation etches both {111} and {100} plane, although the {111} plane is more easily etched than the {100} plane.

Typical FE-SEM images of the pristine non-doped diamond and BDD electrodes are shown in **Fig. 2.3**(a-c), and low-magnification images are shown in **Fig. 2.4**(a-c). The BDD(800) electrode consists of randomly oriented crystallites with both cubic {100} and triangular {111} planes exposed on the surface. The cubic {100} planes appear as regions with slightly brighter contrast compared to the triangular {111} planes in the FE-SEM images obtained with secondary electrons due to different electron affinity [27-29]. The brighter-contrasted cubic {100} regions gradually disappear as the B/C ratio increases. At the maximum boron content of 5000 ppm, the surface is dominated by triangular {111} planes. The preferential orientation was also confirmed with XRD (shown in **Fig. 2.5**). The

ratio of the peak intensity of (111) to (400) was $I(111)/I(400)$ = 1.2, 2.8, and 4.2 for boron concentration of 800, 2500, and 5000 ppm (shown in **Fig. 2.5)**, which indicates that the pristine BDD with higher boron content has a more {111} oriented structure. These observations are in accordance with literature data [26].

Typical FE-SEM images of steam-activated BDDs are shown in **Fig. 2.3**(a'-c'), and low-magnification images are shown in **Fig. 2.4**(a'-c'). The degree of etching increases with increased boron concentration. The a-BDD(800) electrode shows evidence of partial etching of the surface, while nanometer-size pits can be observed throughout the surface of a-BDD(5000). In the case of a-BDD(800), both smooth and roughened surfaces are observed. The cubic {100} surface of a-BDD(800) and a-BDD(2500) is smooth and seems to be unaffected by steam activation. On the other hand, etching of the {111} planes is obvious. The majority of the pits were trigon or deformed trigon in shape (shown with arrows), which most likely reflects the atomic arrangement of the {111} planes.

The FE-SEM images show that under the conditions applied, the {111} planes are preferentially etched, and BDD with higher boron concentration is etched to a higher degree since the amount of {111} planes are more abundant. The observed preferential etching of {111} planes is in good accordance with the studies on the steam activation of BDD (1300 ppm boron) electrodes at various activation temperatures (700, 800 and 900 °C) [17], where triangular pits and islands were observed for BDD treated at 700 °C and a highly porous structure with a columnar texture was obtained at 900 °C. In this study, BDD with higher boron content was etched more than that with lower boron content under the same steam-activation conditions. The preferential etching may be due to a higher reactivity of {111} planes compared to {100} or boron may act as pit initiation sites. As a

comparing experiment, steam activation of non-doped diamond film was conducted. In **Fig. 2.3**(d), the diamond film consists of randomly oriented crystallites with both cubic {100} and triangular {111} planes exposed on the surface. After steam activation (**Fig. 2.3**(d')), the {111} planes are preferentially etched, forming many trigon pits in the size of 50-100 nm on the surface. The trigon pits with the wall having many steps can be observed. However, {100} planes show a smooth surface. Thus, preferential {111} etching of BDD surface with steam activation is due to the higher reactivity of {111} compared to {100} planes in the diamond structure.

Raman spectroscopy was conducted to probe the microstructural changes induced by steam activation (**Fig. 2.6**). The assignment of the Raman peaks are summarized in **Table 2.1**. The broad peak at 500 cm^{-1} (peak A) is known to be related to the phonon scattering by boron induced structural modifications [31], and thus can be used to probe any changes in the boron content or environment with steam activation. $I_{disordered\text{-}D}$ is the intensity of the broad peak centered at 1220 cm^{-1} (peak B), which is attributed to disordered diamond structure [1, 31]. I_D is the intensity of the sp^3-bonded carbon in diamond (D band) at 1330 cm^{-1} (peak C). I_G is the intensity of the sp^2-bonded graphitic carbon (G band) at 1580 cm^{-1} (peak D), which is often found as a minor impurity in BDD electrodes prepared by hot-filament assisted chemical vapor deposition [1].

In the case of pristine BDD, a progressive downward shift in wavenumber of peak A from 493 to 467 cm^{-1} is observed with increasing boron concentration in agreement with literature [31]. There is no obvious shift in the position of this peak after steam activation when compared with the respective pristine BDD electrodes at the same level of boron doping (**Table 2.2**). This is a strong indication that the boron concentration in bulk BDD

was unchanged after steam activation; in other words, selective etching of boron seems unlikely.

For pristine BDD, the value of $I_{\text{disordered-D}}/I_D$ and I_D/I_G increases with increase in boron content. The trend in increasing $I_{\text{disordered-D}}/I_D$ and I_D/I_G with increasing boron content is in good agreement with previous reports [26, 32, 33]. After steam activation, $I_{\text{disordered-D}}/I_D$ and I_D/I_G are more or less unchanged (**Table 2.2**). Overall, it can be said that the steam-activation process does not affect the bulk composition in the film, at least within resolution of Raman spectroscopy.

XPS was acquired to study the change in the near surface composition as a result of steam activation. As shown in **Fig. 2.7**, the C1s peak for pristine BDD can be decomposed into five components. The main C1s peak is composed of two components centered at 283.5 and 284.0 eV, which can be attributed to mono-hydrogenated surface (C-H sp^3) and diamond-like carbon (C-C sp^3), respectively [34, 35]. The peak at 282.7 eV corresponds to graphitic carbon (C-C sp^2) that is often found in BDD prepared by hot filament-assisted chemical vapor deposition. Additional components corresponding to C-O is observed at 285.5 eV and C=O at 287.2 eV [28, 36-40], due to partial atmospheric oxidation [38, 39].

The relative abundance of the five carbon species obtained from **Fig. 2.7** for the pristine BDD is shown in **Fig. 2.8**. The decrease in graphitic carbon (C-C sp^2) from 15 to 6 % with increasing level of boron doping from 800 to 5000 ppm observed in pristine BDD is in agreement with the analysis of I_D/I_G from Raman spectra. The abundance of C-O increases with increasing boron content, while no obvious changes for C=O species can be observed. The increase in C-O with increasing boron doping level was also reported for polycrystalline BDD [38, 40]. After steam activation, the relative amount of diamond-like

carbon (C-C sp^3) increased, which correlates to the removal of graphitic impurity (C-C sp^2) (**Fig. 2.7**). C-H sp^3 decreased dramatically, while the amount of C-O increased as a result of steam activation. The amount of C-O in a-BDD is higher for higher boron content, reflecting the higher degree of etching.

The change in surface area of BDD after steam activation was probed electrochemically. **Fig. 2.9** shows cyclic voltammograms of BDD electrodes before and after steam activation in 0.5 M H_2SO_4 between −0.2 and 0.8 V vs Ag/AgCl. The electrical double layer capacitance per geometric surface area for the pristine BDD shows a slight increase with increase in boron concentration (**Table 2.3**). This phenomenon has been attributed to surface defects induced by boron doping, providing more electrochemically active sites, which in turn increases the electrical double layer capacitance [41]. After steam activation, a clear increase in electrical double layer capacitance is observed, indicating an enlargement in the electrochemically active surface area. The enhancement factor is more pronounced for BDD with higher boron concentration, reaching 838 µF cm^{-2} for a-BDD(5000), 17.5 times higher compared to BDD(5000). The voltammograms tend to tilt for steam-activated BDD with higher boron concentration, which is an artifact of the higher surface area. In order to take into account of the enhancement in the roughness, the current density was normalized by the capacitance (j / C). The capacitance-normalized cyclic voltammograms are all comparable as shown in **Fig. 2.9**(B). Thus, it can be said that the steam activation does not have any negative effect on the bulk conductivity of BDD, i.e., the steam-activation process does not induce any increase in bulk electrode resistance.

Cyclic voltammograms recorded in a wide potential range (−1.0 to 2.5 V vs Ag/AgCl) are shown in **Fig. 2.10**. In addition to the increase in electrochemically active surface area, a wider potential window, one of the most important aspects of BDD electrodes, was observed after steam activation. Here the potential window is defined as the potential where $\Delta j\ \Delta E^{-1}\ C^{-1}$ is below 25 mA mF^{-1} V^{-1}, where C is the capacitance measured between −0.2 and 0.8 V vs Ag/AgCl and ΔE is 40 mV. The potential windows for various electrodes estimated in this manner are shown in **Fig. 2.10**(B) and summarized in **Table 2.3**. The potential window for the a-BDD(800) at 800 °C for 2 h was 3.34 V, appreciably larger than that for pristine BDD of 2.64 V. The increase is attributed to the removal of sp^2-bonded graphitic carbon that limits the potential window.

Based on the obtained knowledge, the preferential etching mechanism is proposed as shown in **Fig. 2.11**. The ideal diamond surface prior to exposure is terminated with hydrogen atoms. The hydrogen abstraction from the surface is a result of the heat treatment, which leads to carbon atom with a dangling bond and sp^3-bonds with neighboring carbon atoms formed on diamond surface. These dangling bonds provide sites of enhanced reactivity. The hydrogen atoms on the {111} surface are more reactive than those on the (2×1) restructured {100} plane (as shown in **Chapter 1**, Page 2), which leads to easier oxidation of {111} than {100} [24]. During heat treatment, H_2O can release an active O atom easily at high temperature [42]. The active O atom adsorbed at dangling bond result into the formation of atop O atom. For {100} planes, surface trend to form ether (C-O-C) with one incoming O, making the surface carbon atoms unattractive to incoming O atoms. Once oxidation, the {100} planes reach its steady state and seems difficult to further oxidation [24]. The {111} surface has a significant number of carbon atoms with dangling bond, result into more active O atom. The incoming O atom collide

with an atop O atom, pushing it aside. The force of the collision broke a C-C bond, with the incoming O atom adding itself to the surface, forming an ether. Another C-C bond broken followed by an O-C ether bond broken. Finally, a C-C bond broke, releasing a CO_2 molecule. When second and third diamond layer break, the sp^2 carbon formed that can be removed quickly, leading to the removal of carbon atom from {111} plane [23].

The macroscopic view of the steam activation of BDD with different boron content is schematically illustrated in **Fig. 2.12**. BDD with low boron content consists of cubic {100} and triangular {111} orientated planes exposed on the surface. Triangular {111} planes dominate the surface of BDD with high boron content. During steam activation at 800 °C, the removal of graphitic carbon from the surface occurs first, followed by the etching of {111} planes. For the steam-activated BDD with low boron content, the {111} planes are easily corroded, whereas, no etching behavior occurs on the {100} planes. In the case of BDD with high boron doping with the surface dominated by {111} planes, the etching occurs homogeneously throughout the surface of the film, inducing a heavily etched surface with trigonal pits. As a result, BDD with higher boron content showed a higher surface area after steam activation compared to BDD with low boron content.

2.4. Summary

Steam activation of BDD electrodes with different levels of boron doping was conducted in order to gain more insight into the steam-activation process. The preliminary control experiment with non-diamond crystallites shows that steam activation etches both {111} and {100} plane, although the {111} plane is more easily etched than the {100} plane. The surface of BDD with 800 ppm boron consists of randomly oriented crystallites with cubic {100} and triangular {111} planes. After steam activation at 800 °C, selective etching of the {111} planes could be realized on the surface of steam-activated BDD (800 ppm B). On the other hand, BDD with 5000 ppm boron, which is dominated by triangular {111} planes, was heavily etched by steam activation forming many nanometer-size pits on the surface. The increase in electrical double layer capacitance was observed after steam activation, and the enhancement factor was more pronounced for BDD with higher boron concentration. A 17.5 times increase in roughness was obtained by steam-activation of BDD with 5000 ppm B. Steam activation at 800 °C etches the {111} planes, but does not corrode the {100} planes. The study of non-doped diamond film indicates that the boron is probably not the active site for etching. The preferential etching mechanism was discussed based on the obtained results, indicating that {111} have higher reactivity compared to {100} planes against steam activation. The higher capacitance (surface area) obtained for BDD with higher boron content is attributed to the higher fraction of {111} planes exposed on the surface. Steam activation is an effective method to increase the active surface area of BDD electrodes and at the same time, enlarge the potential window by removing graphitic impurities. Steam-activated BDD electrode is anticipated to be advantageous for electrolysis applications.

References

[1] A. Fujishima, Y. Einaga, T. N. Rao and D. A. Tryk, Diamond Electrochemistry, Tokyo: Elsevier Amesterdam-BKC; 2005.

[2] E. Brillas and C. A. Martínez-Huitle, Synthetic Diamond Films: Preparation, Electrochemistry, Characterization and Applications, John Wiley & Sons; 2011.

[3] J. L. Davidson, W. D. Brown, A. Gicquel, B. V. Spitsyn and J. C. Angus, Diamond Materials VI. New York: *The Electrochemical Society*; 1999.

[4] J. Iniessta, P. A. Michaud, M. Panizza, G. Gerisola, A. Aldaz and C. Conmninellis, *Electrochim. Acta*, **46**, 3573 (2001).

[5] N. Katsuki, E. Takahashi, M. Toyoda, T. Kurosu, M. Iida and S. Wakita, *J. Electrochem. Soc.*, **145**, 2358 (1998).

[6] M. Shizuno, K. Nakanishi, M. Inaba, M. Uno, Y. Nishiki and T. Furuta, *ECS Trans.*, **16**, 1 (2009).

[7] K. Honda, T. N. Rao, D. A. Tryk, A. Fujishima, M. Watanabe and K. Yasui, *J. Electrochem. Soc.*, **148**, A668 (2001).

[8] Y. Takasu, S. Konishi, W. Sugimoto and Y. Murakami, *Electrochem. Solid-State. Lett.*, **9**, C114 (2006).

[9] T. Ohashi, W. Sugimoto and Y. Takasu, *Electrochim. Acta*, **54**, 5223 (2009).

[10] A. Ahmadpour and D. D. Do, *Carbon*, **34**, 471 (1996).

[11] F. Rodríguez-Reinoso, M. Molina-Sabio and M. T. González, *Carbon*, **33**, 15 (1995).

[12] M. Molina-Sabio, M. T. Gonzalez, F. Rodriguez-Reinoso and A. Sepiijlveda-Escribano, *Carbon*, **34**, 505 (1996).

[13] A. Linares-Solano, C. Salinas-Martínez de Lecea, D. Cazorla-Amorós and I. Martín-Gullón, *Energy & Fuels*, **14**, 142 (2000).

[14] J. Pastor-Villegas and C. J. Durán-Valle, *Carbon*, **40**, 397 (2000).

[15] S. Romá, J. F. González, C. M. González-García and F. Zamora, *Fuel Process. Technol.*, **89**, 715 (2008).

[16] J. F. González, S. Román, C. M. González-García, J. M. Valente Nabais and A. Luis Ortiz, *Ind. Eng. Chem. Res.*, **48**, 7474 (2009).

[17] T. Ohashi, J. Zhang, Y. Takasu and W. Sugimoto, *Electrochim. Acta*, **56**, 5599 (2011).

[18] T. Evans and H. Sauter, *Philos. Mag.*, **6**, 429 (1961).

[19] F. K. de Theije, N. J. van Der Laag, M. Plomp and W. J. P. van Enckevort, *Philos. Mag. A.*, **80**, 725 (2000).

[20] F. K. de Theije, O. Roy, N. J. V. de Laag and W. J. P. van Enckevort, *Diamond Relat. Mater.*, **9**, 929 (2000).

[21] F. K. de Theije, E. V. Veenendaal, W. J. P. van Enckevort and E. Vileg, *Surf. Sci.*, **492**, 91 (2001).

[22] Z. Shpilman, I. Gouzman, E. Grossman, L. Shen, T. K. Minton and J. P. Paci, *J. Phys. Chem. C*, **114**, 18996 (2010).

[23] J. T. Paci, G. C. Schatz and T. K. Minton, *J. Phys. Chem. C*, **115**, 14770 (2011).

[24] J. T. Paci, T. K. Minton and G. C. Schatz, *Acc. Chem. Res.*, **45**, 1973 (2012).

[25] Y. Fedortchouk, D. Canil and E. Semenets, *Am. Mineral.*, **92**, 1200 (2007).

[26] K. Ushizawa, K. Watanabe, T. Ando, I. Sakaguchi, M. Nishitani-Gamo and Y. Sato, *Diamond Relat. Mater.*, **7**, 1719 (1998).

[27] E. Gheeraert, P. Gonon, A. Deneuville, L. Abello and G. Lucazeau, *Diamond Relat. Mater.*, **2**, 742 (1998).

[28] P. Wurzinger, P. Pongratz, P. Hartmann, R. Haubner, B. Lux, *Diamond Relat. Mater.*, **6**, 763 (1997).

[29] C. H. Goeting, F. Marken, A. Gutiérrez-Sosa, R. G. Compton and J. S. Foord, *Diamond Relat. Mater.*, **9**, 390 (2000).

[30] Z. Zheng, H. Kanda, T. Ohasawa and S. Yamaoka, *J. Mater. Sci. Lett.*, **9**, 331 (1999).

[31] F. Pruvost, E. Bustarret and A. Deneuville. *Diamond Relat. Mater.*, **9**, 295 (2000).

[32] P. W. May, W. J. Ludlow, M. Hannaway, P. J. Heard, J. A. Smith and K. N. Rosser, *Diamond Relat. Mater.*, **17**, 105 (2008).

[33] J. W. Ager, W. Walukiewicz, M. McCluskey, M. A. Plano and M. I. Landstrass, *Appl. Phys. Lett.*, **66**, 616 (1995).

[34] N. Simon, H. Girard, M. Manesse, D. Ballutaud and A. Etcheberry, *Diamond Relat. Mater.*, **17**, 1371 (2008).

[35] M. Wang, N. Simon, G. Charrier, M. Bouttemy, A. Etcheberry and M. Li, *Electrochem. Commun.*, **12**, 351 (2010).

[36] D. Ballutaud, T. Kociniewski, J. Vigneron, N. Simon and H. Girard, *Diamond Relat. Mater.*, **17**, 1127 (2008).

[37] S. Ferro, M. D. Colle and A. D. Battisti, *Carbon*, **43**, 1191 (2005).

[38] S. Ghodbane, D. Ballutaud, A. Deneuville and C. Baron, *Phys. Stat. Sol.*, **203**, 3147 (2006).

[39] S. Ghodbane, D. Ballutaud, F. Omnès and C. Agnès, *Diamond Relat. Mater.*, **19**, 630 (2010).

[40] A. F. Azevedo, M. R. Baldan and N. G. Ferreira, *J. Phys. Chem. Solids*, **74**, 599 (2013).

[41] R. Trouillon, D. O'Hare and Y. Einaga, *Phys. Chem. Chem. Phys.*, **13**, 5422 (2011).

[42] R. T. Yang and K. L. Yang, *Carbon*, **23**, 537 (1985).

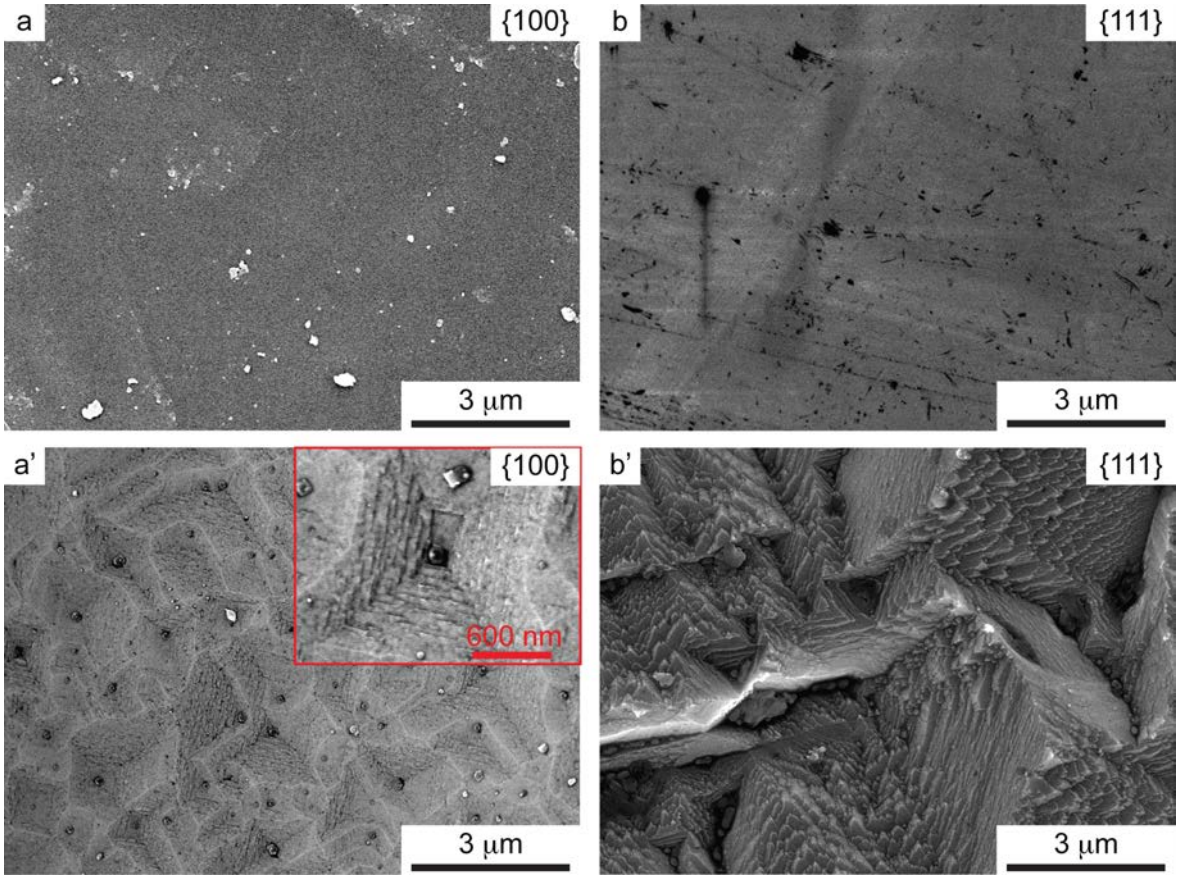

Fig. 2.1. Typical SEM images of {100} and {111} plane of diamond crystallites (a, b) before and (a', b') after steam activation at 900 °C for 2 h.

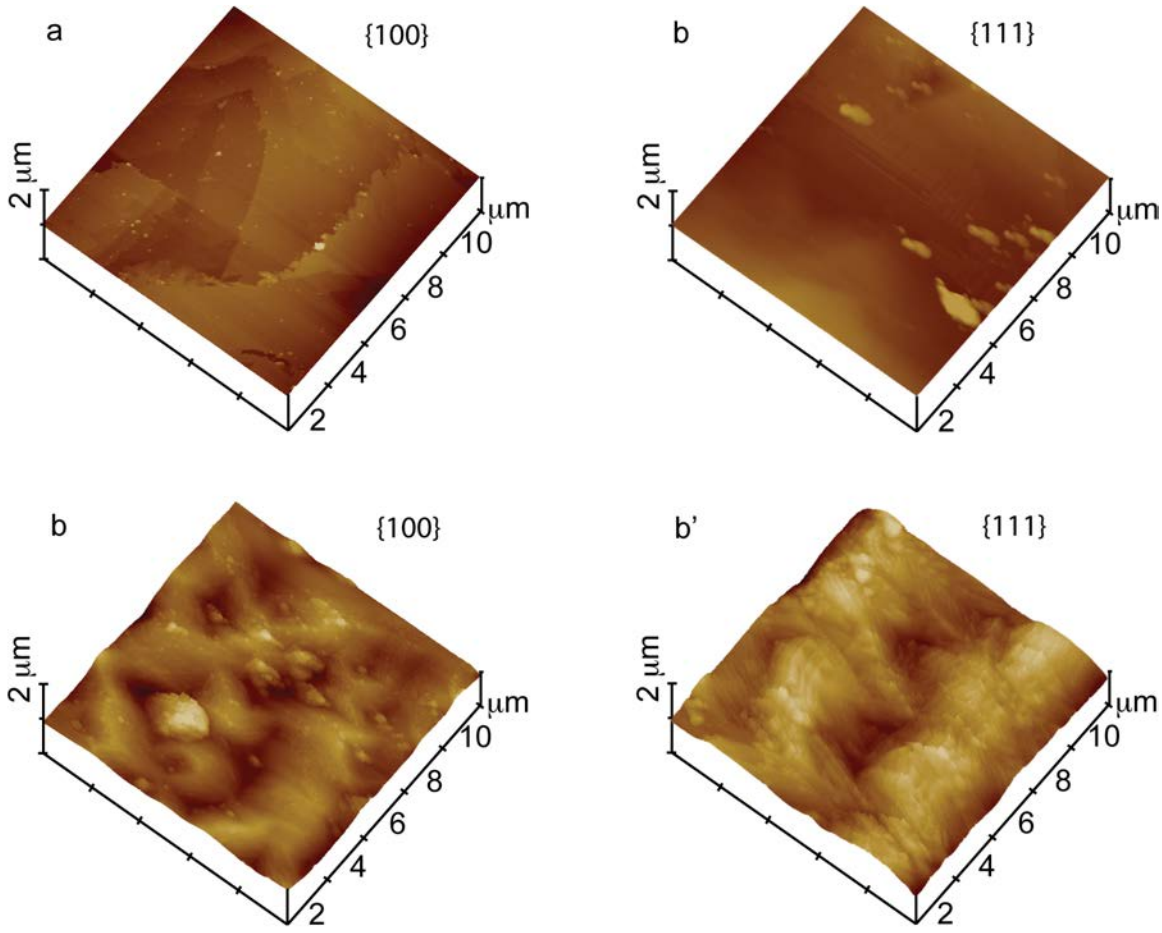

Fig. 2.2. Typical AFM tapping mode images of {100} and {111} plane of diamond crystallites (a, b) before and (a', b') after steam activation at 900 °C for 2 h.

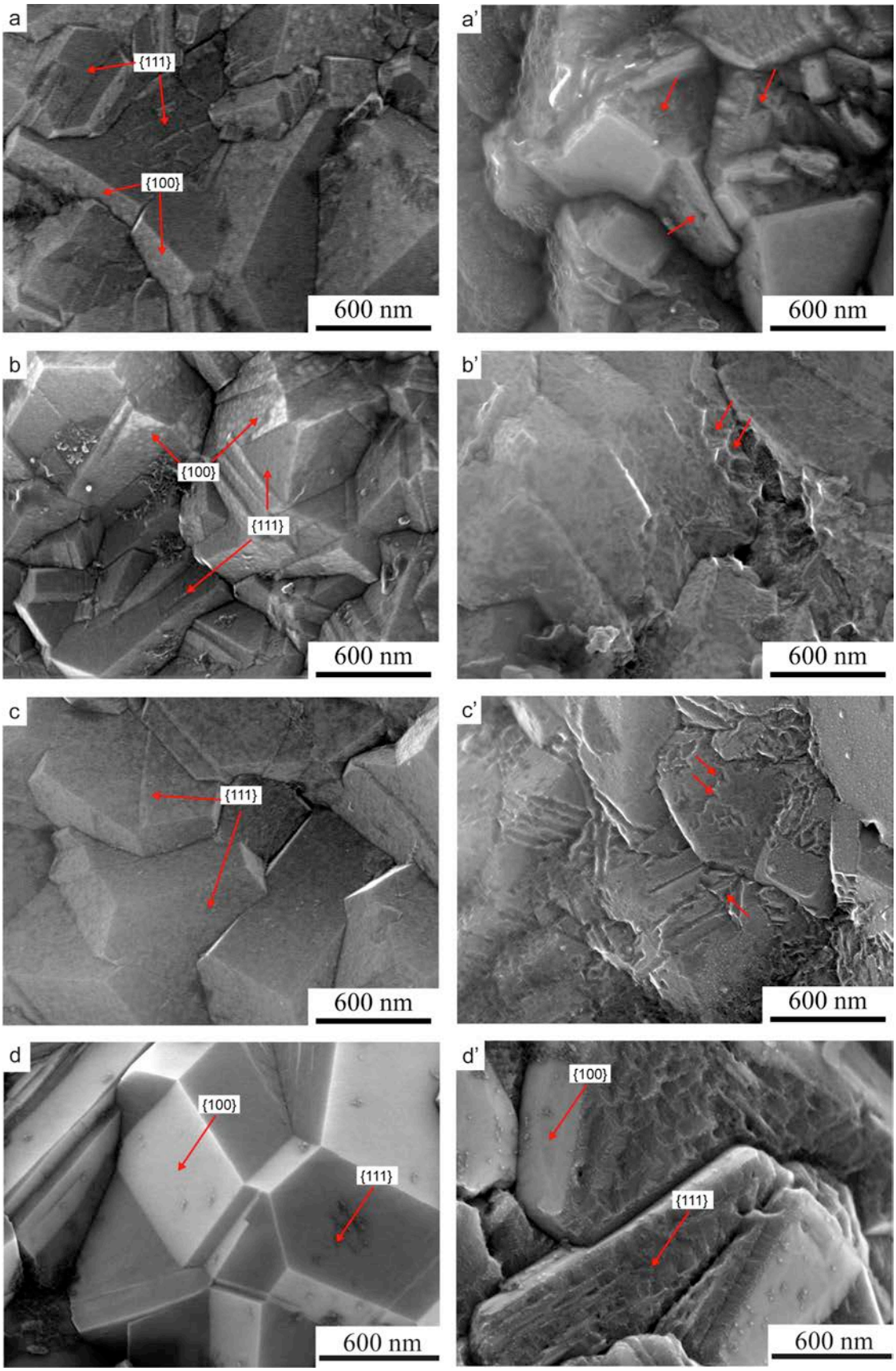

Fig. 2.3. Typical HR-SEM images of pristine BDD with boron content of (a) 800, (b) 2500 and (c) 5000 ppm. Respective images of steam-activated BDD with (d) 800, (e) 2500 and (f) 5000 ppm boron. (d) and (d') are the images of non-doped diamond film before and after steam activation, respectively.

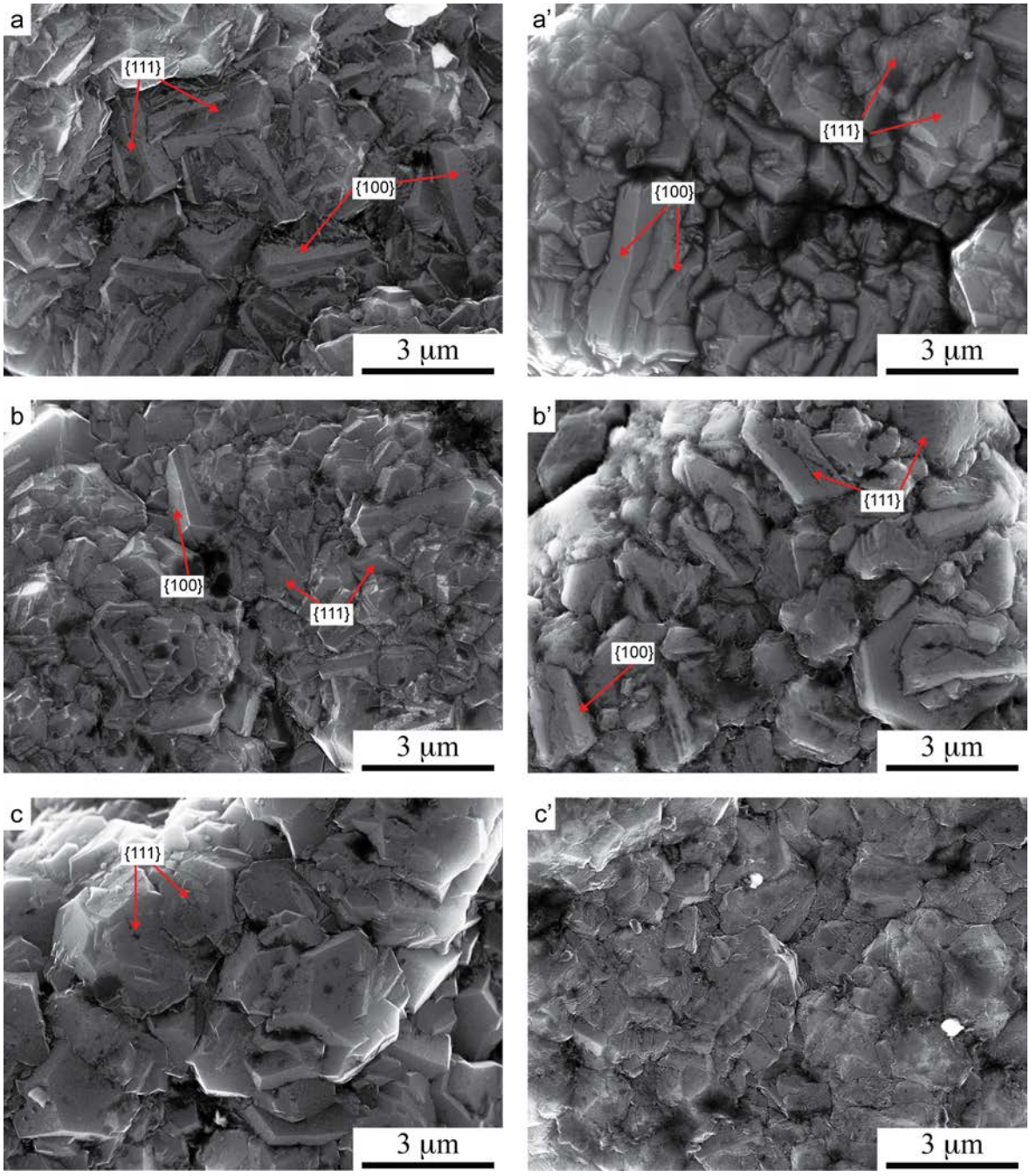

Fig. 2.4. Typical low-magnification HR-SEM images of pristine BDD with boron concentration of (a) 800, (b) 2500 and (c) 5000 ppm. Respective images of steam-activated BDD with (a') 800, (b') 2500 and (c') 5000 ppm.

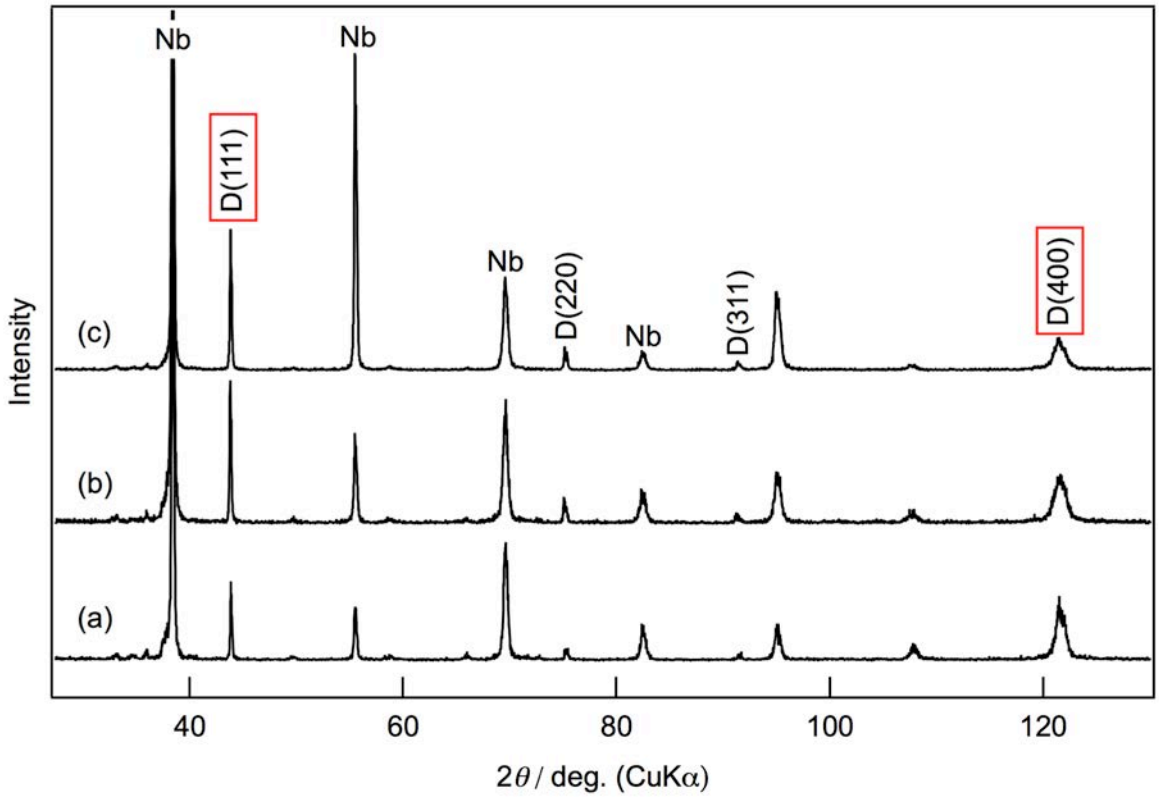

Fig. 2.5. XRD patterns for pristine BDD with boron concentration of (a) 800 ppm, (b) 2500 ppm and (c) 5000 ppm.

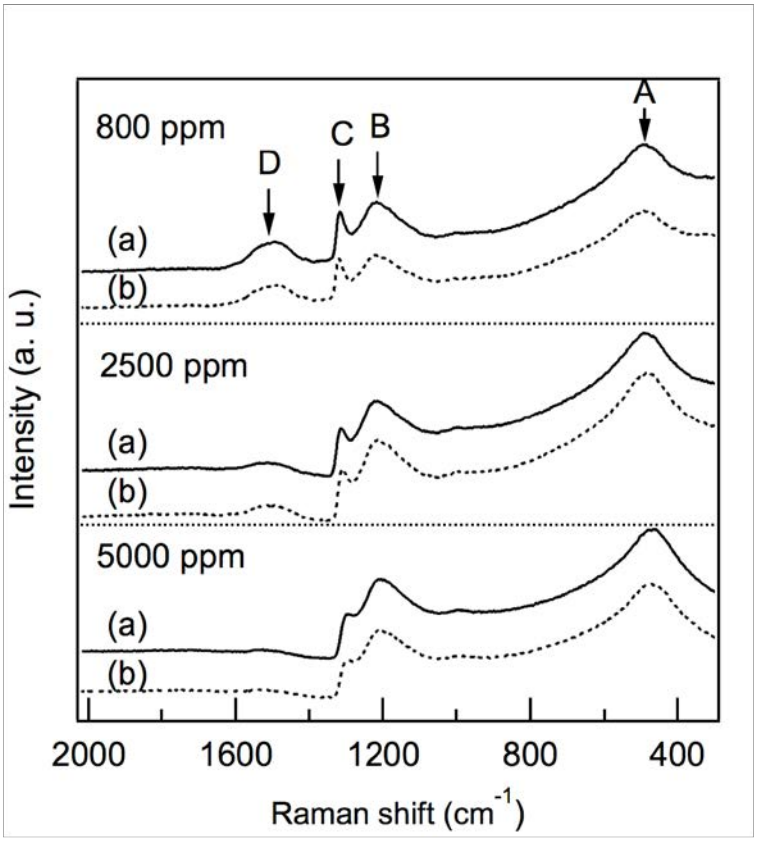

Fig. 2.6. Raman spectra of (a) pristine BDD and (b) steam-activated BDD with different boron content (800, 2500, 5000 ppm).

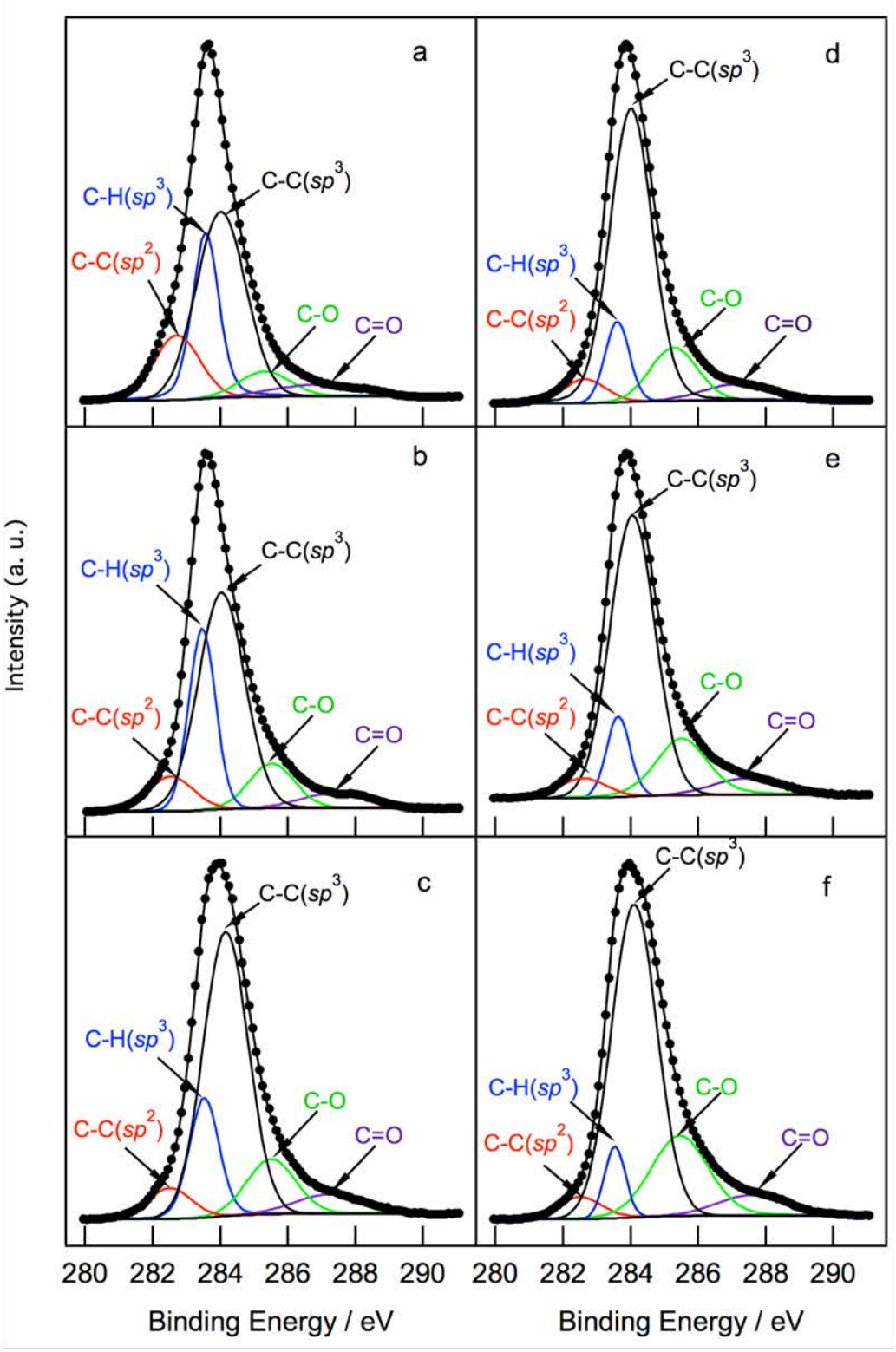

Fig. 2.7. C1s spectra of pristine BDD with boron content of (a) 800, (b) 2500 and (c) 5000 ppm. Respective spectra of steam-activated BDD with (d) 800, (e) 2500 and (f) 5000 ppm.

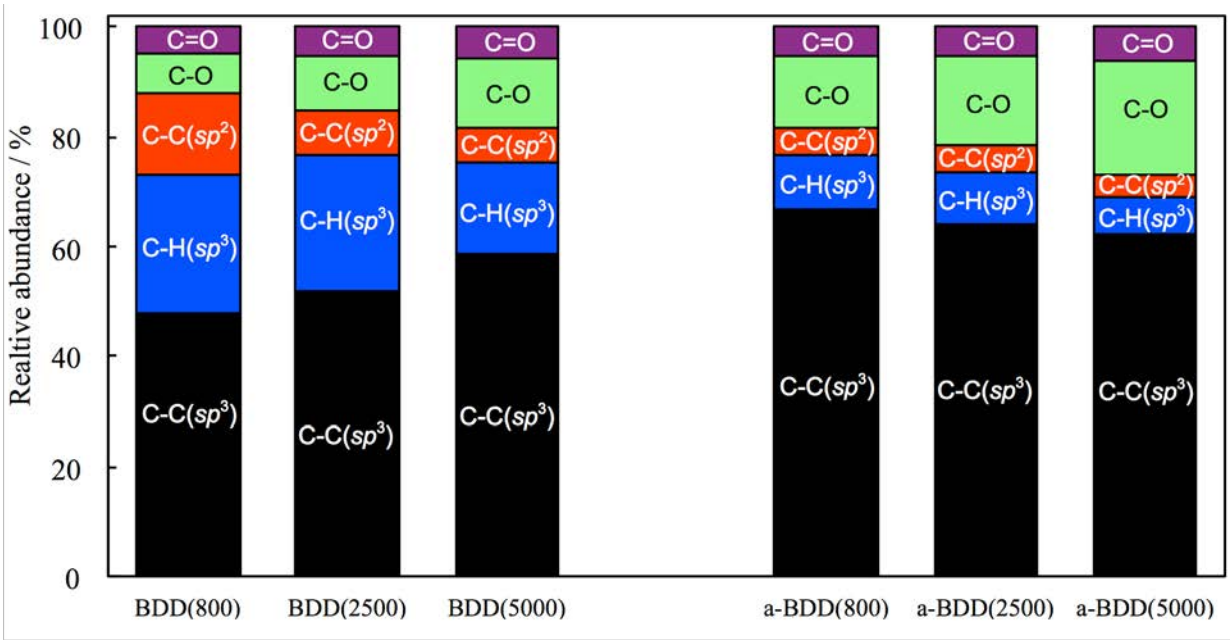

Fig. 2.8. Relative abundance of the carbon species on BDD surface before and after steam activation based on XPS (from **Fig. 2.7**).

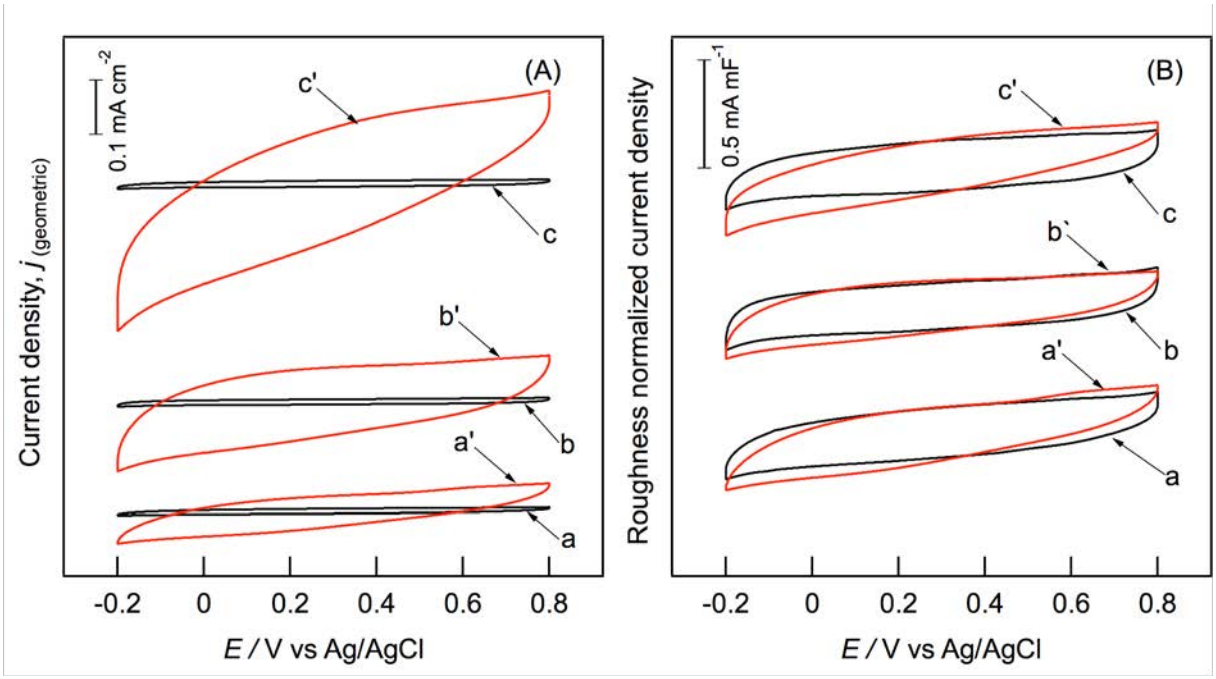

Fig. 2.9. (A) Cyclic voltammograms of BDD electrodes at 100 mV s^{-1} in 0.5 M H_2SO_4 between −0.2 and 0.8 V vs Ag/AgCl (sat. KCl) for (a) BDD(800), (a') a-BDD(800), (b) BDD(2500), (b') a-BDD(2500), (c) BDD(5000) and (c') a-BDD(5000). (B) Voltammograms from (A) with the current taking into account of the enhancement in roughness.

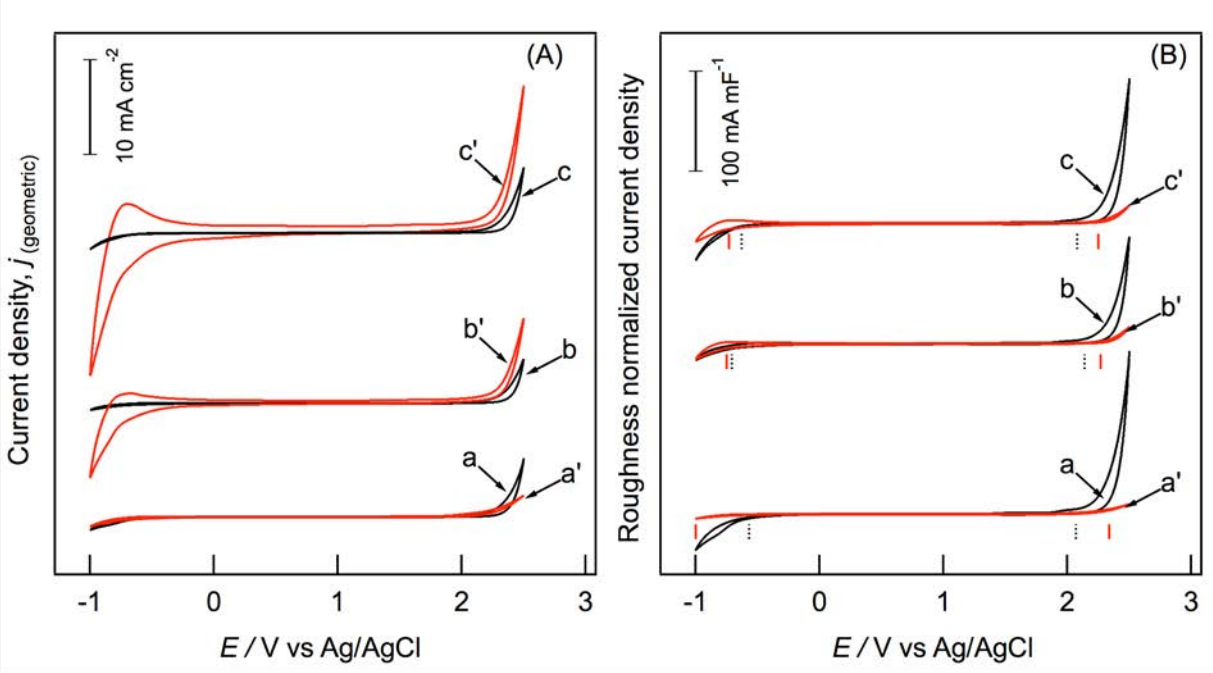

Fig. 2.10. (A) Cyclic voltammograms of BDD electrodes at 100 mV s^{-1} in 0.5 M H_2SO_4 between −1 and 2.5 V vs Ag/AgCl (sat. KCl) for (a) BDD(800), (a') a-BDD(800), (b) BDD(2500), (b') a-BDD(2500), (c) BDD(5000) and (c') a-BDD(5000). (B) Voltammograms from (A) with the current taking into account of the enhancement in roughness.

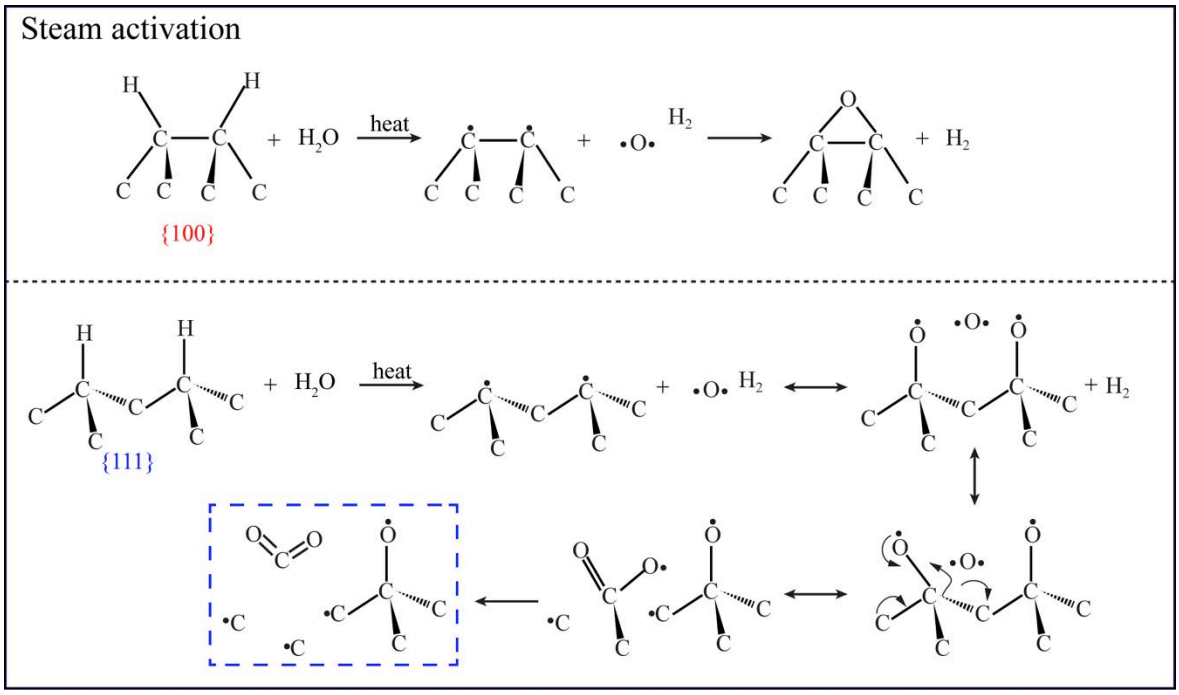

Fig. 2.11. Proposed etching mechanism of diamond {111} and {100} plane by steam activation.

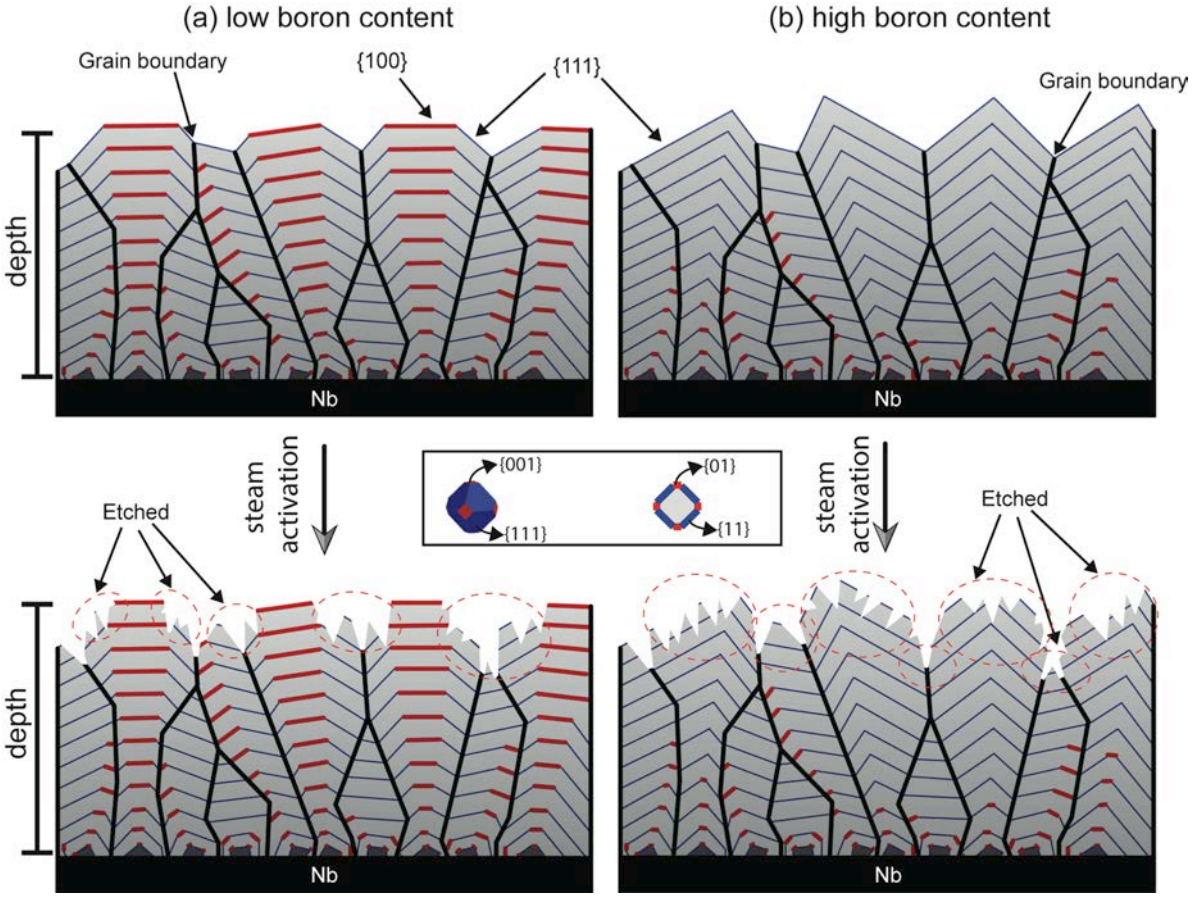

Fig. 2.12. Schematic illustration of the steam-activation process of BDD electrode with (a) low and (b) high boron content.

Table 2.1. Assignment of Raman peaks in **Figure 2.6**.

Label	Raman shift / cm^{-1}	Characteristic species in the film
A	500	Associated with the boron dopant atoms
B	1220	Disordered diamond
C	1330	sp^3-bonded diamond carbon (D-band)
D	1580	sp^2-bonded graphitic carbon (G-band)

Table 2.2. Selected properties of pristine BDD and steam-activated BDD with different boron concentration from Raman spectra.

BDD electrodes		Raman shift of peak A / cm^{-1}	I_D/I_G (a)	$I_{disordered\text{-}D}/I_D$ (b)
800 ppm B	Pristine	493	2.6	1.17
	Activated	490	2.8	1.10
2500 ppm B	Pristine	482	3.7	1.59
	Activated	483	3.4	1.55
5000 ppm B	Pristine	467	5.3	1.81
	Activated	465	5.0	1.80

(a) The peak intensity ratio of the sp^3-bonded carbon (D band) to the sp^2-bonded carbon (G band) in diamond.

(b) The peak intensity ratio of the disordered sp^3-bonded carbon to the sp^3-bonded carbon (D band).

Table 2.3. Electrochemical properties of pristine BDD and steam-activated BDD with different boron content.

BDD electrodes		Specific capacitance /μF $cm^{-2}_{geometric}$	Enhancement factor [(a)] /−	Potential window [(b)] /V vs Ag/AgCl (sat. KCl)
800 ppm B	Pristine	38	−	−0.57 − 2.07
	Activated	225	5.9	<−1.00 − 2.34
2500 ppm B	Pristine	44	−	−0.71 − 2.14
	Activated	525	11.9	−0.75 − 2.27
5000 ppm B	Pristine	48	−	−0.63 − 2.08
	Activated	838	17.5	−0.73 − 2.25

(a) The geometric capacitance of steam-activated electrodes normalized by the geometric capacitance of the respective pristine BDD.

(b) The potential window is defined as the potential region where $\Delta j\ \Delta E^{-1}\ C^{-1} < 25$ mA $mF^{-1}\ V^{-1}$ (ΔE = 40 mV).

Chapter 3

Preferential {100} etching of boron-doped diamond electrodes by CO_2 activation

3.1. Introduction

The etching of diamond has been studied for both from fundamental standpoints [1-7] as well as for practical applications in conductive BDD electrodes [8-13]. The oxidative etching of diamond with O_2 and O_2/H_2O, as well as thermal and hyperthermal atomic oxygen have indicated that the {100} planes are more erosion resistant compared to the {111} planes [1-7]. In **chapter 2**, a similar phenomenon was observed in the case of H_2O etching of conductive boron-doped and non-doped diamond, where steam activation leads to preferential etching of the {111} planes. In addition to O_2 and H_2O, CO_2 is also a common oxidative etchant. CO_2 activation has been widely used to prepare activated carbon, and is known to lead to activated carbon with a different microstructure compared to steam activation [14-19]. CO_2 activation produce an opening, followed by widening of microporosity, while steam activation widens the microporosity from the early stage of the process, the resulting activated carbon has a wide pore size distribution. Despite the abundant work on the preparation of activated carbon via CO_2 and steam activation, information on the reaction between CO_2 and diamond is scarce. The oxidative etching of diamond in kimberlite melts at high temperatures and high pressures have shown that oxidation of diamond with CO_2 and H_2O produce different surface features on {111} and {100} faces, suggesting that the relative oxidation rate is different for H_2O and CO_2 and is also sensitive to the diamond plane [20, 21]. To the best of our knowledge, the reaction between CO_2 and boron-doped diamond has not been studied yet. These studies motivated us to study the CO_2 activation of boron-doped diamond. In contrast to the {111} etching observed by steam activation in boron-doped diamond, CO_2 activation is anticipated to lead to preferential etching of the boron-doped {100} planes.

Polycrystalline BDD is grown on substrates mainly by CVD processes and consists of randomly oriented crystallites with a mixture of cubic {100} and triangular {111} orientated planes exposed on the surface. Since electro-catalysis and redox reactions are both surface sensitive, BDD with preferential planes exposed to the surface would contribute to a better understanding of the kinetics and electrochemical activity of BDD surfaces. The ratio of the exposed planes in BDD electrodes is governed by the CVD conditions and is not easily controlled. For example, highly boron-doped BDD are composed mainly of {111} faces, thus it is difficult to grow diamond films with {100} orientation with high levels of boron doping. The higher level of boron doping in {111} has been suggested to be the cause of higher electron transfer kinetics for redox couples such as $[Ru(NH_3)_6]^{2+/3+}$ and $[Fe(CN)_6]^{3-/4-}$ for {111} than {100} [22, 23].

In this chapter, CO_2 activation is conducted on polycrystalline boron-doped diamond film composed of a mixture of {111} and {100} planes, as well as non-doped diamond to investigate the etching behavior on boron-doped diamond (BDD) surfaces.

3.2. Experimental section

Boron-doped (800 ppm) diamond films were synthesized by hot filament-assisted chemical vapor deposition on a Nb substrate (2×2 cm^2) following previously procedures [24, 25]. The electrode with the BDD layer facing up was positioned in a silica boat and set in a silica furnace tube. The furnace temperature was raised to the activation temperature at a rate of 5 °C min^{-1} under flowing N_2 (99.99995 %). When the activation temperature was reached, N_2 gas was changed to CO_2 gas (200 mL min^{-1}) and held for 2 h. Finally, the samples were cooled down to room temperature under flowing N_2. The samples will be denoted as a-BDD(800°C) and a-BDD(900°C) for BDD activated at 800 and 900 °C, respectively. CO_2 activation of non-doped diamond films and crystallites was conducted in a similar manner for BDD electrodes. Activation process was conducted in an open system with the outlet gas exposed to atmospheric pressure.

A field emission-scanning electron microscope (FE-SEM; Hitachi S-5000) was used for morphological observation. Atomic force microscopy (Bruker, Digital Instruments Nanoscope III ADC 5) was performed in air using silicon cantilevers (Bruker, NCHV-A) and a 130 μm scanner (AS-130V). X-ray photoelectron spectroscopy (XPS) was performed on a Kratos Axis Ultra DLD X-ray photoelectron spectrometer with spectral resolution of approximately 0.8 eV using a standard Mg Kα (1256.6 eV) X-ray source operated at 15 mA and 15 kV. All binding energies were referenced to Au ($4f_{7/2}$) at 83.7 eV. The C1s spectra were fitted with asymmetric mixed Gaussian-Lorentzian sum functions using the XPS peak fitting software XPSpeak (version 4.1). The microstructure of BDD was characterized by Raman spectroscopy (Kaiser Optical Systems, Inc., Raman Microscope System 3000) with a YAG laser (excitation wavelength 532 nm) as the excitation source.

3.3. Results and discussion

As a preliminary control experiment, non-doped diamond crystallites were subjected to CO_2 activation for gaining a macroscopic insight into the activation process. As shown in **Fig. 3.1**(a), the {100} plane is rigorously etched with square pits (around 200 - 400 nm) with pit density of 5.7 pits μm^{-2}. Etching of the {111} plane is less obvious with some point-bottomed trigons in the size of 100-300 nm (**Fig. 3.1**(b)). The trigonal pit density (0.1 pits μm^{-2}) is similar to the defect density of pristine diamond {111} plane (**Fig. 2.10**(b) in **Chapter 2**), suggesting that the etching occurs at the defect sites. The surface roughness (*R*) was obtained from AFM images (**Fig. 3.2**). Before activation, the roughness is $R < 10$ nm for both {111} and {100} planes (**Fig. 2.2**(a, b) in **Chapter 2**). After CO_2 activation, increase in roughness of only the {100} plane ($R = 102$ nm) is apparent, and no obvious change can be observed for {111} plane ($R = 10$ nm). CO_2 activation leads to preferential etching of {100} and the {111} plane is resistant to activation, which is the opposite of what has been observed in the case of steam activation.

The pristine BDD (800 ppm boron) electrode consists of randomly oriented crystallites with a mixture of cubic {100} and triangular {111} orientated planes exposed on the surface, as shown in **Fig. 3.3**(a and a'). The {100} and {111} planes can be identified by their shape as well as the difference in contrast in the FE-SEM images. In FE-SEM images obtained with secondary electrons, the cubic {100} planes appear as regions with slightly brighter contrast compared to the triangular {111} planes due to different electron affinity [26]. Some inhomogeneity in the contrast is observed on the {100} surface, which may suggest inhomogeneity in the partial atmospheric oxidation of the surface.

A typical FE-SEM image of BDD after CO_2 activation at 800 °C is shown in **Fig. 3.3**(b and b'). For a-BDD(800°C), numerous nanopits (5-10 nm) can be observed on the {100} planes, while no etching is evident on the {111} planes, which is more clearly seen in images with higher magnification (**Fig. 3.4**). As a comparing experiment, CO_2 activation was also conducted on the non-doped diamond film at 800 °C. As shown in **Fig. 3.5**, the mild etching of {100} planes forms numerous nanopits (5-10 nm), while no obvious etching occurs on the {111} plane. Since the similar etching behavior was observed for both CO_2-activated non-doped and boron-doped diamond film, we presume that boron is probable not active site for etching.

FE-SEM images of a-BDD(900°C) reveals that progressive etching of the {100} planes at 900 °C forms larger square pits with size of 200-400 nm along the crystal edges (shown with red arrows in **Fig. 3.3**(c and c')), resulting in a macro-porous texture. Etching is so severe at 900 °C, that the {111} planes are no longer able to be distinguished after CO_2 activation. In the case of activated carbon, CO_2 first produces narrow micropores and then the pores are widened as activation progresses [14-19]. If the mechanism of CO_2 activation of BDD is similar to that of activated carbon, then the activation at 900 °C can be attributed to the widening of the nanopits to form large (200-400 nm) square pits.

Raman spectroscopy was employed to probe the microstructure of the BDD film before and after CO_2 activation (**Fig. 3.6**), and the selected properties are shown in **Table 3.1**. Peak A at around 500 cm^{-1} is known to shift with the level of boron doping, and the broad peak B centered at 1220 cm^{-1} is attributed to the disordered diamond structure (disordered-D). The zone-center optical phonon of diamond (D-band) appears at 1330 cm^{-1} (Peak C). The sp^2-bonded graphitic carbon (G-band) is observed at 1580 cm^{-1} (peak D),

which is often found as a minor impurity in BDD electrodes prepared by hot-filament assisted chemical vapor deposition. After CO_2 activation, no shift can be observed for peak A. The ratio of the intensity of D-band to G-band (I_D/I_G) and disordered-D to D-band ($I_{disordered\text{-}D}/I_D$) are used to investigate microstructure changes of BDD film. For a-BDD(800°C), I_D/I_G and $I_{disordered\text{-}D}/I_D$ are more or less unchanged as compared to the pristine BDD within resolution of Raman spectroscopy (**Table 3.1**). For a-BDD(900°C), the significant increase in I_D/I_G and decrease in $I_{disordered\text{-}D}/I_D$ indicates the removal of the non-diamond impurities by CO_2 activation.

XPS data was acquired to investigate the change in the carbon species on the surface of BDD (**Fig. 3.7**). The relative abundance of the five carbon species obtained from the XPS data is shown in **Fig. 3.8**. The percentage of C-C(sp^2) decrease from 8.2 % for pristine BDD to 4 - 5 % for the CO_2-activated BDD, indicating the removal of graphitic impurity by CO_2 activation. This observation was also supported by Raman spectroscopy. Oxygen functional groups (C-O, C=O) in pristine BDD are due to partial atmospheric oxidation. After CO_2 activation at 800 °C, the relative abundance of C=O increase from 5.6 % to 7.7 % without any obvious change in the C-O. CO_2 activation at 900 °C leads to a further increase in C=O content to 9.2 % and an increase in C-O from 11.8 % to 15.2 % compared to the pristine BDD. The abundance of C-H decreases from 23.7 % for the pristine BDD to 8.8 % for CO_2 activated BDD at 900 °C. C=O is known to form on the {100} plane after oxidation of hydrogen-terminated diamond [27, 28]. A similar trend has been reported for anodic oxidation of BDD, producing C-O and C=O on the {100} plane, while C-O is generated on the {111} plane [29]. Coupled with the FE-SEM images showing the preferential etching of the {100} plane, the increase in C=O can thus be associated to the partial oxidation of the {100} plane. Although the conditions of oxidation

are different, the trend in the kinetics of oxidation by CO_2 activation seems to be similar to oxidation of diamond and anodic oxidation of BDD.

Based on the obtained knowledge, the possible CO_2-activation mechanisms for diamond {111} and {100} plane are proposed in **Fig. 3.9**. Heat treatment results into the hydrogen abstraction from the surface, which leads to carbon atom with a dangling bond and sp^3-bonds with neighboring carbon atoms forming on diamond surface. These dangling bonds provide sites of enhanced reactivity. CO_2 is difficult to release O atom during heating [30]. CO_2 adsorbed at dangling bond resulted into the formation of atop O atom, releasing CO molecular. The top O atoms on {111} plane react with CO reversely, generating CO_2. The distance between atop O atoms on the {100} plane is shorter than that on the {111} plane. Thus, the neighbor atop atoms on the {100} collide with each other easily, forming C=O groups or releasing a CO_2, which leads to the removal of carbon atom from {100} plane.

The macroscopic view of the CO_2 activation process of BDD is schematically illustrated in **Fig. 3.10**. CO_2 activation at 800 °C leads to mild etching of {100} planes, forming numerous nanopits (5 - 10 nm) on the {100} plane. When the activation temperature is raised to 900 °C, progressive etching of {100} plane occurs with widening of the pores, resulting in the formation of large square pits (200 - 400 nm) along the crystal edges.

3.4. Summary

CO_2 activation of boron-doped diamond (BDD) and non-doped diamond was conducted. To the best of our knowledge, this is the first study on the CO_2 activation of boron-doped diamond under atmospheric pressure. The preliminary experiment on diamond crystallites also shows that CO_2 activation leads to preferential etching of {100} and the {111} plane is resistant to activation. For BDD electrodes, preferential etching of {100} planes was observed for CO_2 activation at 800 °C, forming numerous nanopits (5 - 10 nm). At this temperature, etching of the {111} surface is minimal. When the activation temperature was set to 900 °C, a macroporous BDD surface composed of 200 - 400 nm pits was obtained. The study on CO_2 activation of non-doped diamond film at 800 °C, indicates that the boron is active site for etching. The mechanism was discussed based on the microscopy and XPS analysis, which indicates that the {100} has higher structure sensitivity than {111} against CO_2 activation. Preferential etching behavior of boron-doped and non-doped diamond is the opposite of what has been observed in the case of steam activation. The obtained results may allow one to fabricate BDD electrodes with different exposed surfaces at the same doping level, which is difficult to achieve under typical CVD procedures.

Reference

[1] T. Evans and H. Sauter, *Philos. Mag.*, **6**, 429 (1961).

[2] F. K. de Theije, N. J. van Der Laag, M. Plomp and W. J. P. van Enckevort, *Philos. Mag. A.*, **80**, 725 (2000).

[3] F. K. de Theije, O. Roy, N. J. van Der Laag and W. J. P. van Enckevort, *Diamond Relat. Mater*., **9**, 929 (2000).

[4] F. K. de Theije, E. van Veenendaal, W. J. P. van Enckevort and E. Vileg, *Surf. Sci*., **492**, 91 (2001).

[5] Z. Shpilman, I. Gouzman, E. Grossman, L. Shen, T. K. Minton and J. T. Paci, *J. Phys. Chem. C*, **114**, 18996 (2010).

[6] J. T. Paci, G. C. Schatz and T. K. Minton, *J. Phys. Chem. C*, **115**, 14770 (2011).

[7] J. T. Paci, T. K. Minton and G. C. Schatz, *Acc. Chem. Res.*, **45**, 1973 (2012).

[8] H. Masuda, T. Yanagishita, K. Yasui, K. Nishio, I. Yagi, T. N. Rao, and A. Fujishima, *Adv. Mater*., **13**, 247 (2001).

[9] C. Terashima, K. Arihara, S. Okazaki, T. Shichi, D. A. Tryk, T. Shirafuji, N. Saito, Osamu Takai and A. Fujishima, *ACS Appl. Mater. Interfaces*, **3**, 177 (2011).

[10] N. Yang, H. Uetsuka, E. Osawa and C. E. Nebel, *Nano Lett.*, **8**, 3572 (2008).

[11] Y. Takasu, S. Konishi, W. Sugimoto and Y. Murakami, *Electrochem. Solid-State Lett.*, **9**, C114 (2006).

[12] T. Ohashi, W. Sugimoto and Y. Takasu, *Electrochim. Acta*, **54**, 5223 (2009).

[13] T. Ohashi, J. Zhang, Y. Takasu and W. Sugimoto, *Electrochim. Acta*, **56**, 5599 (2011).

[14] F. Rodríguez-Reinoso, M. Molina-Sabio and M. T. González, *Carbon*, **33**, 15 (1995).

[15] M. Molina-Sabio, M. T. Gonzalez, F. Rodriguez-Reinoso and A. Sepiijlveda-Escribano, *Carbon*, **34**, 505 (1996).

[16] A. Linares-Solano, C. Salinas-Martínez de Lecea, D. Cazorla-Amorós and I. Martín-Gullón, *Energy & Fuels*, **14**, 142 (2000).

[17] J. Pastor-Villegas and C. J. Durán-Valle, *Carbon*, **40**, 397 (2000).

[18] S. Romá, J. F. González, C. M. González-García and F. Zamora, *Fuel Process. Technol.*, **89**, 715 (2008).

[19] J. F. González, S. Román, C. M. González-García, J. M. Valente Nabais and A. Luis Ortiz, *Ind. Eng. Chem. Res.*, **48**, 7474 (2009).

[20] Y. Fedortchouk, D. Canil and E. Semenets, *Am. Mineral.*, **92**, 1200 (2007).

[21] Y. Fedortchouk, M. H. Manghnani, A. Hushur, A. Shiryaev and F. Nestola, *Am. Mineral.*, **96**, 1768 (2011).

[22] Yu. V. Pleskov, Y. E. Evstefeeva, V. P. Varnin and I. G. Teremetskaya, *Russ. J. Electrochem.*, **40**, 1023 (2004).

[23] Yu. V. Pleskov, Y. E. Evstefeeva, M. D. Krotova, V. P. Varnin and I. G. Teremetskaya, *J. Electroanal. Chem.*, **595**, 168 (2006).

[24] S. Hattori, M. Doi, E. Takahashi, T. Kurosu, M. Nara and S. Nakamatsu, *J. Appl. Electrochem.*, **33**, 85 (2003).

[25] N. Katsuki, E. Takahashi, M. Toyoda, T. Kurosu, M. Iido and S. Wakita, *J. Electrochem. Soc.*, **145**, 2358 (1998).

[26] K. Ushizawa, K. Watanabe, T. Ando, I. Sakaguchi, M. Nishitani-Gamo and Y. Sato, *Diamond Relat. Mater.*, **7**, 1719 (1998).

[27] P. E. Pehrrsson and T. W. Mercer, *Surf. Sci.*, **460**, 74 (2000).

[28] P. E. Pehrrsson and T. W. Mercer. *Surf. Sci.*, **460**, 49 (2000).

[29] T. Kondo, K. Honda, D. A. Tryk and A. Fujishima, *J. Electrochem. Soc.*, **152**, E18 (2005).

[30] M. F. Irfan, M. R. Usman, and K. Kusakabe, *Energy*, **36**, 12 (2011).

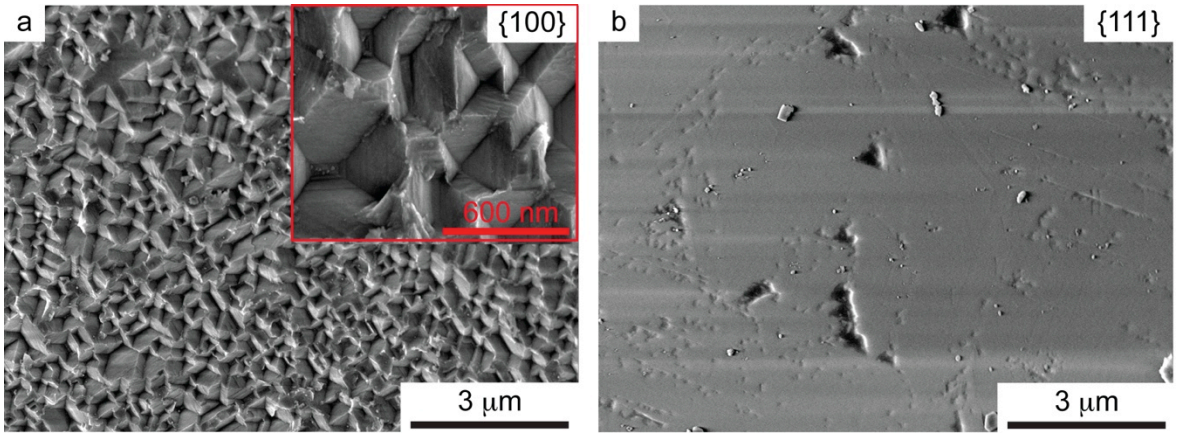

Fig. 3.1. Typical SEM images of (a) {100} and (b) {111} plane of diamond crystallites after CO_2 activation at 900 °C for 2 h.

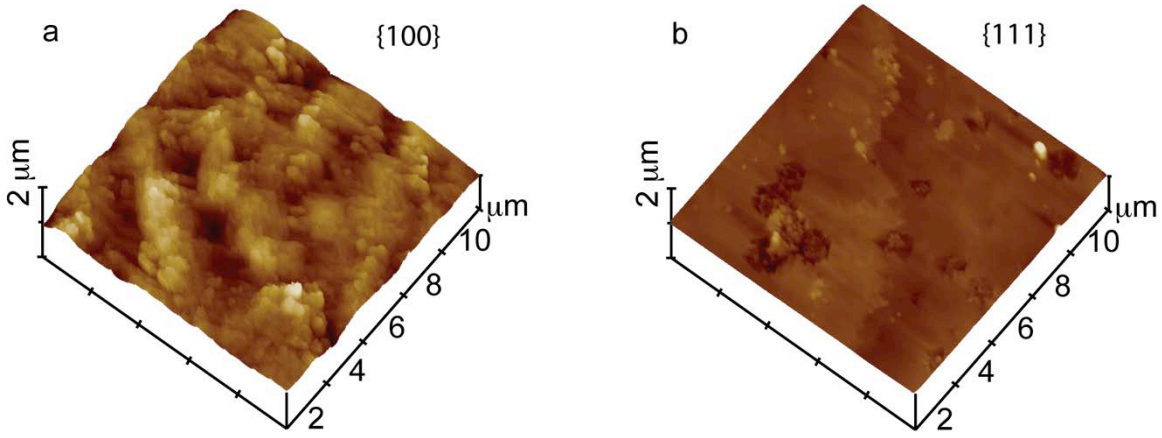

Fig. 3.2. Typical AFM tapping mode images of (a) {100} and (b) {111} plane of diamond crystallites after CO_2 activation at 900 °C for 2 h.

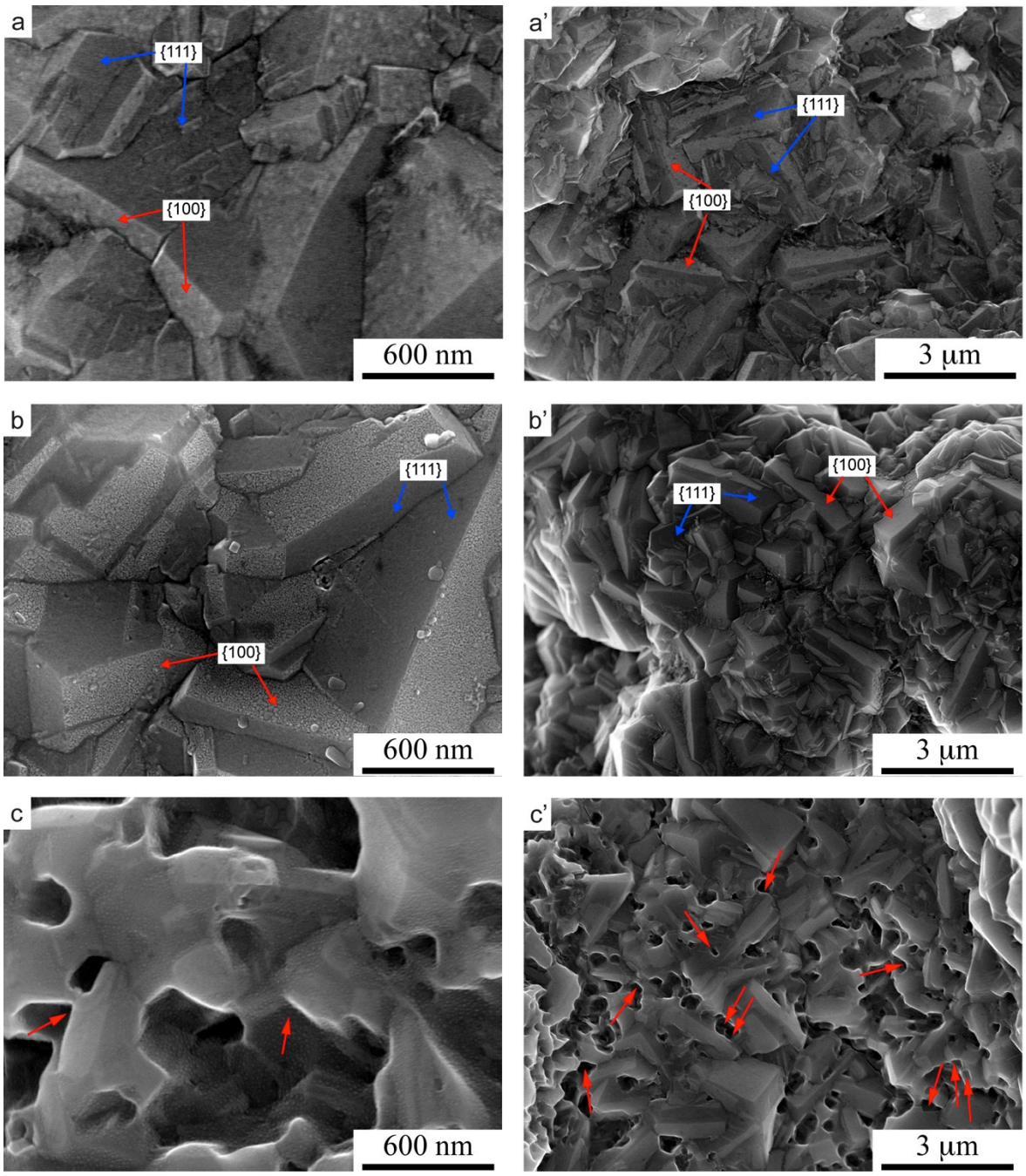

Fig. 3.3. Typical HR-SEM images of (a) pristine BDD, CO_2-activated BDD at (b) 800 °C and (c) 900 °C, respectively. (a'), (b') and (c') are the respective low-magnification images.

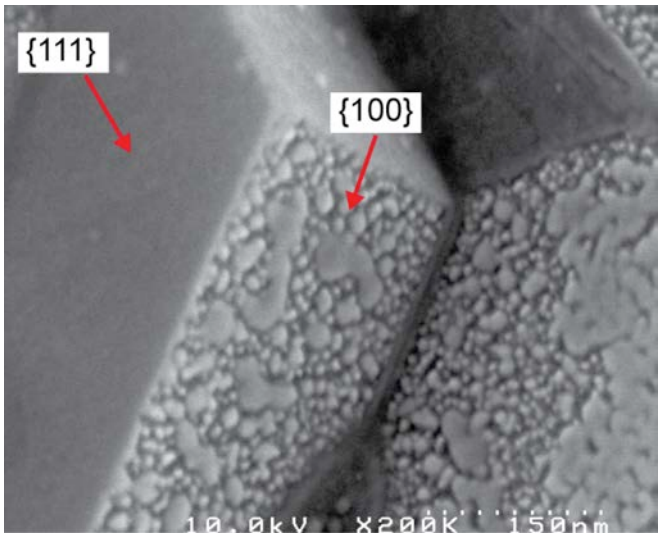

Fig. 3.4. Enlarged image of CO_2-activated BDD at 800 °C.

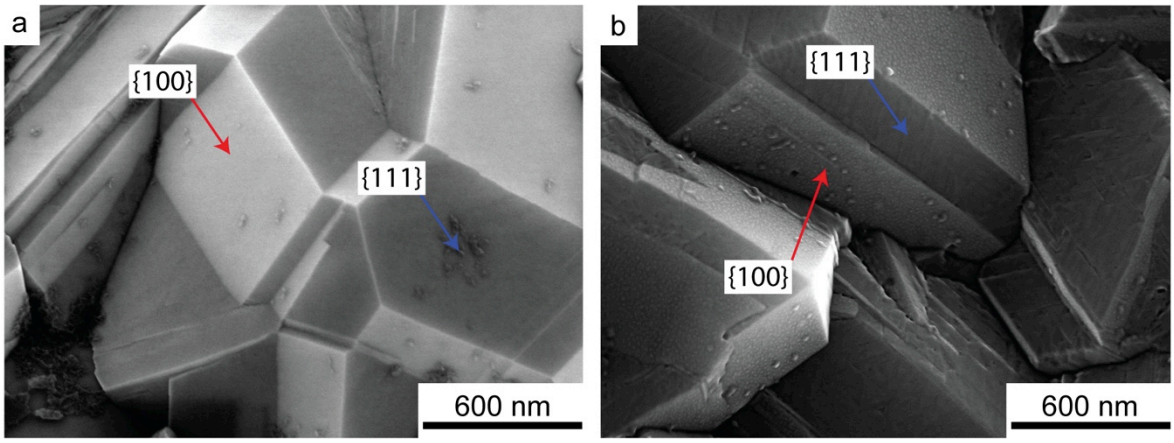

Fig. 3.5. Typical SEM images of non-doped diamond film (a) before and (b) after CO_2 activation at 800 °C for 2 h.

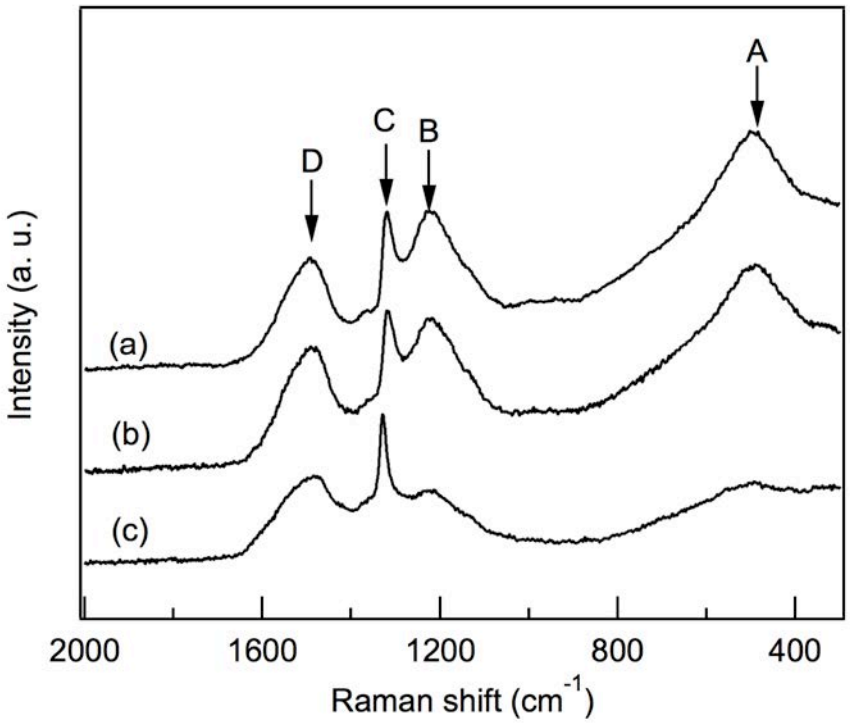

Fig. 3.6. Raman spectra of (a) pristine BDD, CO_2-activated BDD at (b) 800 °C and (c) 900 °C, respectively.

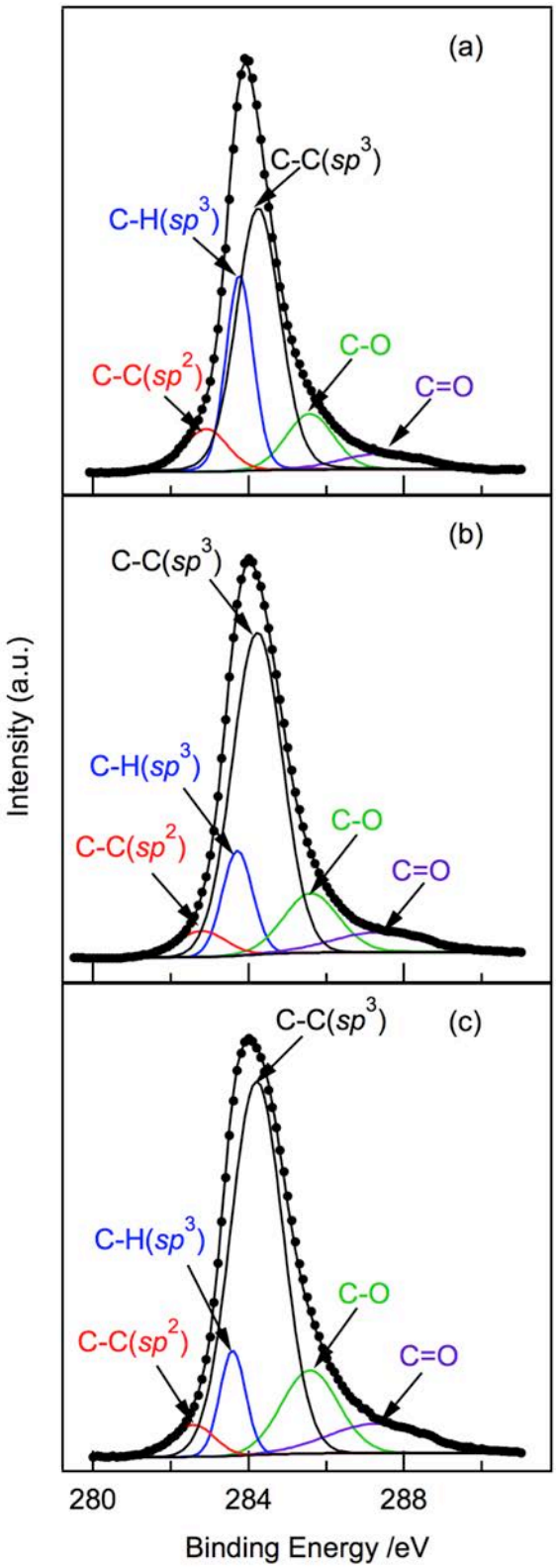

Fig. 3.7. C1s spectra of (a) pristine BDD and CO_2-activated BDD electrodes at (b) 800 °C and (c) 900 °C for 2 h.

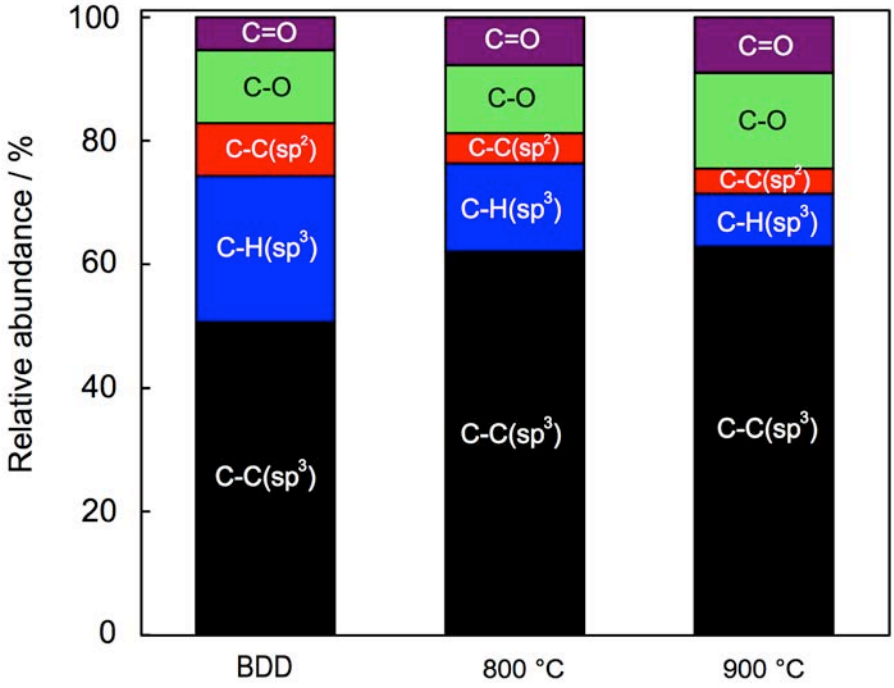

Fig. 3.8. Relative abundance of the carbon species based on XPS analysis on BDD surface.

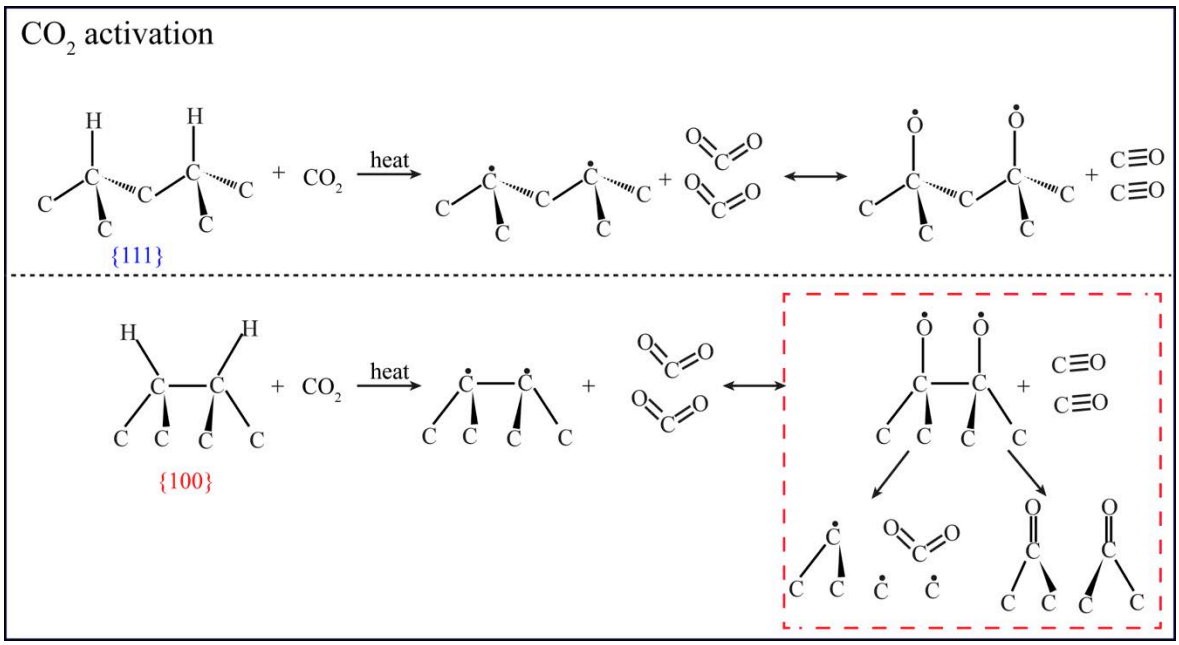

Fig. 3.9. Proposed etching mechanism of diamond {111} and {100} plane by CO_2 activation

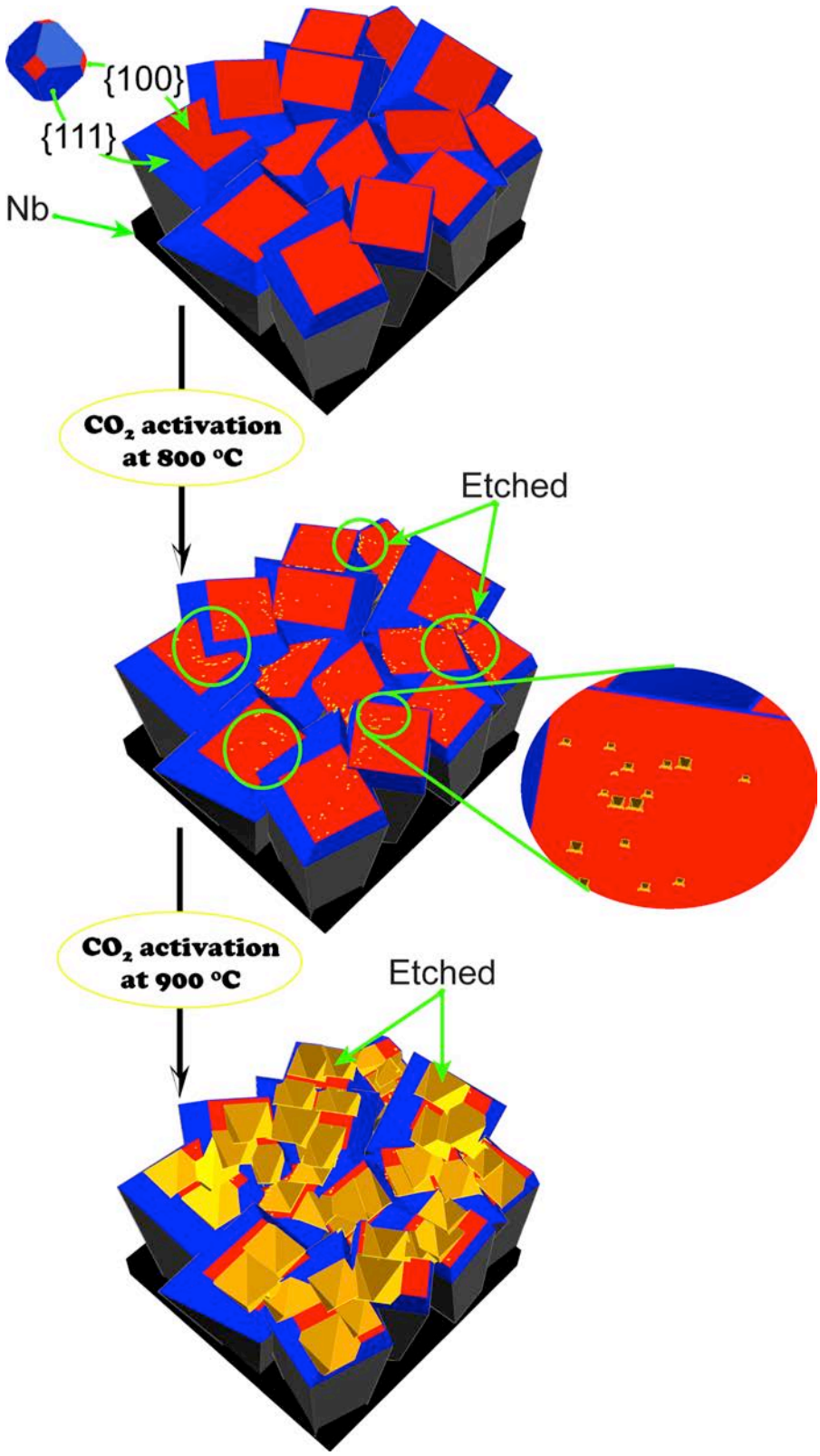

Fig. 3.10. Schematic illustration of the CO_2-activation process of polycrystalline BDD.

Table 3.1. Selected properties of CO_2-activated BDD from Raman spectra.

BDD electrodes	I_D/I_G [(a)]	$I_{disordered\text{-}D}/I_D$ [(b)]	Raman shift of peak A / cm^{-1}
Pristine	1.3	1.00	491
Activated at 800 °C	1.4	0.95	493
Activated at 900 °C	1.8	0.45	491

(a) The peak intensity ratio of the sp^3-donded carbon (D-band) to sp^2-bonded carbon (G-band) in diamond.

(b) The peak intensity ratio of the disordered sp^3-bonded carbon to the sp^3-bonded carbon (D-band).

Chapter 4

Conclusions

Boron-doped diamond film is a novel electrode material, due to its interesting electrochemical properties, such as wide potential window, dimensional stability and low double layer capacitance. Nanostructured BDD surface also attracts much attention for enhanced electrochemical performance. The etching methods have been explored to fabricate BDD electrode with various nanostructures. In this thesis, steam and CO_2 activation were applied to BDD electrodes in an attempt to fabricate porous electrode. The preferential etching behavior was observed for both boron doped and non-doped-diamond, and the mechanism of preferential etching were discussed. This study provides a simple and effective method to control the etching of specific surfaces of sp^3 carbon. The obtained results are summarized below.

In **chapter 1**, the development, electrochemical applications and modification of BDD film were introduced in order to clarify the background of this work.

In **chapter 2**, steam activation of BDD electrodes with different levels of boron doping (800, 2500 and 5000 ppm boron) at 800 °C was conducted, in order to provide detailed insight into the steam-activation process, in particular the effect of boron content. Obtained findings are as follows:

The preliminary control experiment on diamond crystallites shows that steam activation etches both {111} and {100} plane, although the {111} plane is more easily etched than the {100} plane.

After steam activation at 800 °C, preferential etching of the {111} planes could be realized on the surface of steam-activated BDD (800 ppm B). On the other hand, BDD with 5000 ppm boron, which is dominated by triangular {111} planes, was heavily etched by steam activation forming many nanometer-size pits on the surface.

The increase in electrical double layer capacitance was observed after steam activation, and the enhancement factor was more pronounced for BDD with higher boron concentration. A 17.5 times increase in roughness was obtained by steam-activation of BDD with 5000 ppm boron. The higher capacitance (surface area) obtained for BDD with higher boron content is attributed to the higher fraction of {111} planes exposed on the surface.

The study of non-doped diamond film indicates that boron is probably not the active site for etching. The etching mechanism was discussed based on obtained results, which indicates that preferential {111} etching of BDD surface is due to the higher reactivity of {111} compared to {100} planes in the diamond structure.

Steam activation is an effective method to increase the active surface area of BDD electrodes and at the same time, enlarge the potential window by removing graphitic impurities.

In **chapter 3**, CO_2 activation of boron-doped and non-doped diamond was conducted for investigating the etching behavior. This is the first study on the CO_2 activation of boron-doped diamond under atmospheric pressure. The preferential {100} etching of boron-doped diamond is the opposite of what has been observed in the case of steam activation in **chapter 2**. Obtained findings are as follows:

The preliminary control experiment on diamond crystallites shows that CO_2 activation leads to preferential etching of {100} and the {111} plane is resistant to activation.

For BDD electrodes, preferential etching of {100} planes was observed for CO_2 activation at 800 °C, forming numerous nanopits (5 - 10 nm). At this temperature, etching of the {111} surface is minimal. The progressive etching of the {100} planes at 900 °C

forms larger square pits with size of 200-400 nm along the crystal edges, resulting in a macro-porous texture.

The study on CO_2 activation of non-doped diamond film at 800 °C, indicates that the boron is probably not active site for etching. The mechanism was discussed based on the microscopy and XPS analysis, which indicates that the {100} has higher structure sensitivity than {111} against CO_2 activation.

The preferential etching by CO_2 and steam may allow one to fabricate BDD electrodes with different exposed surfaces at the same doping level, which is difficult to achieve under typical CVD procedures.

List of publications

List of publications in the scope of this thesis

○Junfeng Zhang, Takaaki Nakai, Masaharu Uno, Yoshinori Nishiki and Wataru Sugimoto, “Effect of the boron content on the steam activation of boron-doped diamond electrodes”, *Carbon*, **65**, 206-213 (2013).

○Junfeng Zhang, Takaaki Nakai, Masaharu Uno, Yoshinori Nishiki and Wataru Sugimoto, “Preferential {100} etching of boron-doped diamond electrodes and diamond particles by CO_2 activation”, *Carbon*, **70**, 207-214 (2014).

List of publications out of the scope of this thesis

Tatsuya Ohashi, ○Junfeng Zhang, Yoshio Takasu and Wataru Sugimoto; “Steam activation of boron doped diamond electrodes”, *Electrochimica Acta*, **56** (16), 5599-604 (2011).

Acknowledgment

I would like to express the greatest gratitude to my supervisor, Prof. Wataru Sugimoto, for his valuable advise, helpful discussions, and suggestions. This work would never have been completed without his ability to enthusiastically simplify complex problems and his personal encouragement. I am also indebt to Prof. Yasushi Murakami, Prof. Fujio Okino, Prof. Yoshiyuki Hattori and Prof. Soshi Shiraishi (Gunma University) for their many discussions, suggestions, advice and encouragement. Partial financial support from a Grant in-Aid for Global COE Program and Grant in-Aid for Excellent Graduate Schools by the Ministry of Education, Culture, Sports, Science and Technology (MEXT), Japan is appreciated. I also thank my senior collaborator, Dr. Tatsuya Ohashi. I wish to thank Dr. Christophe Chauvin, Mr. Zhongwei Lei and Qingfeng Liu for their many discussions, suggestions and advices. Special thanks go to my collaborators, Yuki Makiuchi. This thesis could not have been completed without their earnest experiments and discussions.

Finally, I thank my parents, wife and older sister for their support, everlasting understanding and love.